

DEVELOPMENT OF RF-POWERED WIRELESS TEMPERATURE SENSOR FOR  
BEARING HEALTH MONITORING

By  
Jhon A. Henao-Sepúlveda

A thesis submitted in partial fulfillment of the requirements for the degree of  
MASTER OF SCIENCES

in

ELECTRICAL ENGINEERING  
UNIVERSITY OF PUERTO RICO  
MAYAGÜEZ CAMPUS  
2004

Approved by:



Rafael Rodríguez Solís, Ph.D.  
Member, Graduate Committee

17 May 2004  
Date



Yi Jia, Ph.D.  
Member, Graduate Committee

May 17, 2004  
Date



Manuel Toledo Quiñones, Ph.D.  
President, Graduate Committee

5/14/2004  
Date



Pedro Resto, Ph.D.  
Representative of Graduate Studies

05/17/04  
Date



Jorge Ortiz Álvarez, Ph.D.  
Chairperson of the Department

May 17, 2004  
Date

## **ABSTRACT**

A battery-less wireless sensing technology to monitor the cage temperature in bearings was developed. Non-contact measurements are necessary because the bearing cage performs a sliding motion with respect to inner and outer races, and its rotation excludes direct wiring and the use of slip rings. Four wireless sensing circuit prototypes were implemented. Three circuits are based on a Colpitts oscillator, a Voltage Controlled Oscillator (VCO) and a Meissner oscillator, respectively, and a fourth sensor is based on Radio Frequency Identification (RFID) principles. Radio-frequency (RF) signals are used to supply the energy to the sensor electronics, so no direct contacts to the sensor circuits are required. Experimental results on a bearing while it is operating are presented. The techniques developed provide a feasible solution for the measurement of the bearing cage temperature, which can be adapted to monitor the condition of other mechanical components for which wired circuits are difficult to use.

## **RESUMEN**

Tecnología de medición inalámbrica sin baterías para monitorear temperatura dentro de rodamientos fue desarrollada en esta tesis. Medidas sin contacto directo con el transductor son necesarias debido a que el complejo movimiento de las partes del rodamiento impide el uso de instrumentación clásica. Se desarrollaron cuatro prototipos experimentales; tres emplean modulación en frecuencia para enviar la información de temperatura usando un oscilador Colpitts, un oscilador controlado por voltaje y un oscilador Meissner, respectivamente. El cuarto emplea el principio de modulación de impedancia. La energía entregada al circuito sensor para su operación fue enviada usando señales de radio frecuencia, así, la potencia y la información son transmitidas en forma inalámbrica sin necesidad de baterías o cableado directo. Resultados experimentales bajo condiciones normales de operación del rodamiento son mostrados. Las técnicas desarrolladas proveen una solución factible para la medición de temperatura en rodamientos y pueden ser adaptadas para monitorear la condición de otros componentes mecánicos.

To my wife and my son  
who have borne my absence  
for all this time.  
I love them

## ACKNOWLEDGEMENTS

I wish to express my gratitude to my advisor Professor Manuel Toledo for his many hours of consultation and discussion which were essential to carry out this thesis; in addition I thank with him for his valuable and friendly guidance and support. I have learned very much from him. I would like to thank to Professor Yi Jia for his great contributions to this work; his knowledge and experience were vital to end this thesis. Another reason that I must acknowledge from his is related to the economic resources that he got for my assistantship and for the thesis financial and for his many hours of discussions dedicated to my thesis. I also wish to thank to Professor Rafael Rodríguez Solís for the time that he dedicated to my thesis, and also to Professor Pedro Resto for his time dedicated to review my thesis as representative of graduate school in my thesis defense. I would like to acknowledge Professors Rogelio Palomera and Manuel Jimenez for allowing me to use the Integrated Circuits Design Laboratory (ICDL). Thanks also to Eduardo Santiago, ICDL administrator, for his unconditional help and friendship, and to my laboratory colleagues and friends (Sandra Ordoñez, José M. Ortiz, José A. García, Sigfredo González, Carlos Vega, José I. López, Ramón Mercado and Gloribel Perez), for making me feel at home during my graduate studies. To all of them thanks.

I would like to thank to Electrical and Computer Engineering, Mechanical Engineering and Industrial Engineering departments for their economic support during my graduate studies. I would also like to thank the financial support from NASA Space grant under IDEAS-ER Project.

# TABLE OF CONTENTS

<b>LIST OF TABLES.....</b>	<b>VIII</b>
<b>LIST OF FIGURES.....</b>	<b>IX</b>
<b>1. INTRODUCTION.....</b>	<b>1</b>
1.1 TEMPERATURE IN BEARING CAGE AS A KEY PARAMETER OF CONDITION MONITORING OF BEARINGS .....	3
1.2 OVERVIEW OF WIRELESS MICRO-SENSORS OPERATED WITH OR WITHOUT BATTERIES.....	6
1.3 SCOPE AND STRUCTURE OF THE THESIS .....	10
<b>2. RF POWER TRANSMISSION FOR WIRELESS SENSORS.....</b>	<b>11</b>
2.1 INDUCTIVE LINK.....	12
2.1.1 Mutual inductance.....	13
2.1.2 Selecting the frequency of operation.....	16
2.1.3 Design and development of inductive link coils .....	17
2.1.4 Inductive link circuit model.....	20
2.2 POWER RECEIVER .....	22
2.2.1 Component selection.....	23
2.2.1.1 LC tank receiver .....	23
2.2.1.2 Rectifier circuit.....	24
2.3 POWER TRANSMITTER .....	24
2.3.1 Driver circuits for inductive links .....	25
2.3.2 Class-E power amplifier design .....	26
2.3.3 Results.....	29
2.4 SUMMARY .....	31
<b>3. TEMPERATURE WIRELESS SENSING CIRCUITS.....</b>	<b>32</b>
3.1 COLPITTS OSCILLATOR – BASED TEMPERATURE SENSOR.....	32
3.1.1 Principle of operation.....	32
3.1.2 Circuit design .....	34
3.2 VOLTAGE CONTROLLED OSCILLATOR – BASED TEMPERATURE SENSOR .....	38
3.2.1 Principle of operation.....	38
3.2.2 Circuit design .....	39
3.3 MEISSNER OSCILLATOR – BASED TEMPERATURE SENSOR.....	43

3.3.1	Principle of operation.....	43
3.3.2	Circuit design .....	44
3.4	RADIO FREQUENCY IDENTIFICATION – BASED TEMPERATURE SENSOR.....	46
3.4.1	Principle of operation.....	46
3.4.2	Circuit design .....	48
3.5	FABRICATION OF THE SENSORS .....	50
3.5.1	Manufacturing process .....	50
3.5.2	Installation of wireless sensors on bearings.....	51
3.6	SUMMARY .....	54
<b>4.</b>	<b>IMPLEMENTATION RESULTS.....</b>	<b>55</b>
4.1	SENSOR CALIBRATION .....	55
4.1.1	Calibration procedure and setup .....	55
4.1.2	Calibration results.....	58
4.2	TEMPERATURE MONITORING ON AN OPERATING BEARING .....	65
<b>5.</b>	<b>CONCLUSIONS .....</b>	<b>69</b>
	<b>BIBLIOGRAPHY.....</b>	<b>72</b>

## LIST OF TABLES

Table 1. Parameters of inductive link coils .....	19
Table 2. Design components of class-E power amplifier.....	29
Table 3. Power efficiency of the system .....	30
Table 4. Full-range Centigrade temperature of LM60 IC-temperature sensor .....	39
Table 5. Comparison between the wireless sensors.....	64
Table 6. Capture range of temperature data for each wireless sensor principle .....	64

## LIST OF FIGURES

Figure 1. Remotely powered wireless temperature sensor (a) Printed circuit implemented (b) bearing instrumented with the sensor.....	2
Figure 2. Experimental tests of the RF-powered wireless temperature monitoring system under real operational conditions of a bearing.....	2
Figure 3. Thermal overheating results on bearings. Taken from [7].....	4
Figure 4. Roller bearing elements. Taken from [10].....	5
Figure 5. Wireless capacitive sensor and electrical equivalent. Taken from [15]. ....	7
Figure 6. Equivalent circuit model of the wireless pressure sensor. Taken from [15].....	7
Figure 7. Inductive powering in medical implants. Taken from [21].....	8
Figure 8. Schematic diagram of the wireless temperature sensor system. ....	10
Figure 9. RF powering principle.....	11
Figure 10. Transformer model for inductive links with a induced voltage ( $V_{ind}$ ).....	12
Figure 11. Mutual inductance between two-coaxial filament loops.....	14
Figure 12. Mutual inductance calculations (a) using model approach of (6) and (b) using model approach of (10).....	16
Figure 13. Mutual inductance as a function of transmitter coil radius (a) using model of equation (6) and (b) using model of equation (10). Receiver coil radius $b=3.5\text{cm}$ .....	19
Figure 14. Schematic of the circuit model for the inductive coupling system.....	20
Figure 15. Secondary (receiver) coil voltage vs. coil distance for both models of mutual inductance and experimental data. (Input voltage: $20 V_{pp}$ at 10 MHz).....	22
Figure 16. Energy receiver circuits. (a) Half bridge configuration and (b) voltage doubler configuration.....	23
Figure 17. Simple class-E tuned power amplifier.....	26
Figure 18. Setup used to measure the received DC voltage as a function of the distance between the coils.....	30
Figure 19: DC Voltage at receiver circuit as a function of the distance between coils.....	31
Figure 20. Schematic for RF-powered wireless temperature sensor based on Colpitts oscillator. ....	33
Figure 21. Temperature behavior for X7R and Y5V dielectric type capacitors. Taken from [53-54].....	34
Figure 22. Colpitts oscillator diagram for component selection. (a) DC analysis and (b) AC analysis.....	35
Figure 23. RF powered wireless temperature sensor using a Colpitts Oscillator.....	36
Figure 24. Block diagram for a wireless temperature system using two Colpitts oscillators.....	37
Figure 25. Power spectrum of a received signal using two Colpitts oscillators configuration.....	37

Figure 26. Connection diagram for LM60 IC-temperature sensor .....	38
Figure 27. VCO implemented with discrete circuit elements. Taken from [57] .....	39
Figure 28. Integrated VCO from MAXIM. Taken from [57].....	40
Figure 29. Schematic diagram for RF-powered wireless temperature sensor based on a Voltage Controlled Oscillator.....	42
Figure 30. RF powered wireless temperature sensor using a Voltage Controlled Oscillator and an IC temperature sensor .....	42
Figure 31. Schematic diagram for wireless temperature sensor based on a Meissner Oscillator..	44
Figure 32. Wireless temperature sensor based on Meissner oscillator. (a) LC sensor unit and (b) amplifier and reception unit.....	45
Figure 33. Circuit model for backscattering modulation technique.....	47
Figure 34. Waveform signal for the backscattering modulation (AM signal).....	47
Figure 35. Schematic diagram for the RF powered wireless system based on RFID principle.....	48
Figure 36. RF-powered wireless temperature sensor based on RFID principle. ....	49
Figure 37. Pattern of a wireless temperature sensor circuit. (a) Eagle Pattern and (b) pattern implementation .....	51
Figure 38. Printed Circuit Board with SMT electronic components.....	52
Figure 39. First version of the RF-powered wireless temperature sensor based on LC Colpitts oscillator installed on a tapered roller bearing.....	52
Figure 40. Latest version of the RF-powered wireless temperature sensor based on LC Colpitts oscillator installed on a tapered roller bearing.....	53
Figure 41. RF-powered wireless temperature sensor based on LC Colpitts oscillator installed on a ball bearing built over a polyimide film.....	54
Figure 42. Sensor calibration setup.....	56
Figure 43. FFT of received signals for temperatures of 25°C (1.160 MHz) and 70°C (1.88 MHz), respectively when using the wireless sensor based on a Colpitts oscillator. ....	57
Figure 44. Display of the Labview program used for temperature data acquisition and analysis .	57
Figure 45. Calibration curve for a wireless temperature sensor based on a Colpitts oscillator .....	59
Figure 46. Temperature and frequency history respectively for calibration of the wireless temperature sensor based on a Colpitts oscillator.....	59
Figure 47. Calibration curve for a wireless temperature sensor based on a VCO .....	60
Figure 48. Temperature and frequency history respectively for calibration of the wireless temperature sensor based on a VCO .....	60
Figure 49. Calibration curve for a wireless temperature sensor based on a Meissner Oscillator ..	61
Figure 50. Temperature and frequency history respectively for calibration of the wireless temperature sensor based on a Meissner oscillator .....	62

Figure 51. Acquired calibration signals for the RF-powered wireless temperature sensor based on RFID principle. (Signals recorded for 23°C, 35° and 90°C respectively).....	63
Figure 52. Calibration curve for the RF-powered wireless temperature sensor based on RFID principle .....	63
Figure 53. Experimental setup for real test of a ball bearing instrumented with an RF-powered wireless temperature sensor.....	66
Figure 54. Bearing temperatures under several rotation speeds and two load conditions.....	66
Figure 55. Cage temperature behavior of the bearing operating at 1200 rpm with a load of (a) 25 pounds and (b) 45 pounds .....	67
Figure 56. Cage temperature behavior of the bearing operating at 1550 rpm with a load of (a) 25 pounds and (b) 45 pounds .....	68

## 1. INTRODUCTION

The present thesis explores the development of wireless technology to monitor the bearing health by means of temperature measurements in the bearing cage. Specifically, the objective is to develop remotely-powered wireless temperature micro-sensors to monitor the temperature variations of the bearing cage. This would enable the detection of damage and prevent catastrophic failures not only in bearing applications but in many systems with rotating elements.

The temperature bearing monitoring systems used in this study consist of a sensor with an electronic transmitter, an external data receiver (an antenna), and a central computer. Temperature sensing elements and the electronic transmitter circuit are located on the bearing cage. Data measured during the bearing operation is wirelessly sent via a modulated carrier signal to an external receiver. To avoid the use of batteries, another radio signal is used to provide power to the sensor circuit.

The bearing temperature monitoring systems (see Figures 1 and 2) developed in this thesis have three main components: an RF power transmitter, an RF power supply (receiver) and a sensing circuit. An inductively coupled link compound of two coils has been used as a mean to supply power to the sensing circuits. Because of this magnetic coupling, the power transmitter induces a voltage in a receiving coil. The transmitter, shown in Figure 2, must provide of the power required by the circuits in the receiving unit to operate. Figure 1(a) shows the wireless sensing system which consists of an RF-power supply and a sensing circuit placed on the same printed circuit board. The RF power supply receives the energy transmitted by the stationary power transmitter and converts it into a DC voltage used for the sensing circuit's operation. The sensing circuit measures and modulates the temperature data captured by a temperature sensitive element. Once designed and implemented on a printed circuit board, the sensing circuit was installed into a bearing, as shown in Figure 1(b). Finally the instrumented bearing was tested under normal operational conditions using the setup showed in Figure 2. An

antenna located in a vicinity of the sensor was used to capture the cage temperature sent by the wireless sensor. The cage temperature was captured by and recorded in a PC.



Figure 1. Remotely powered wireless temperature sensor (a) Printed circuit implemented (b) bearing instrumented with the sensor

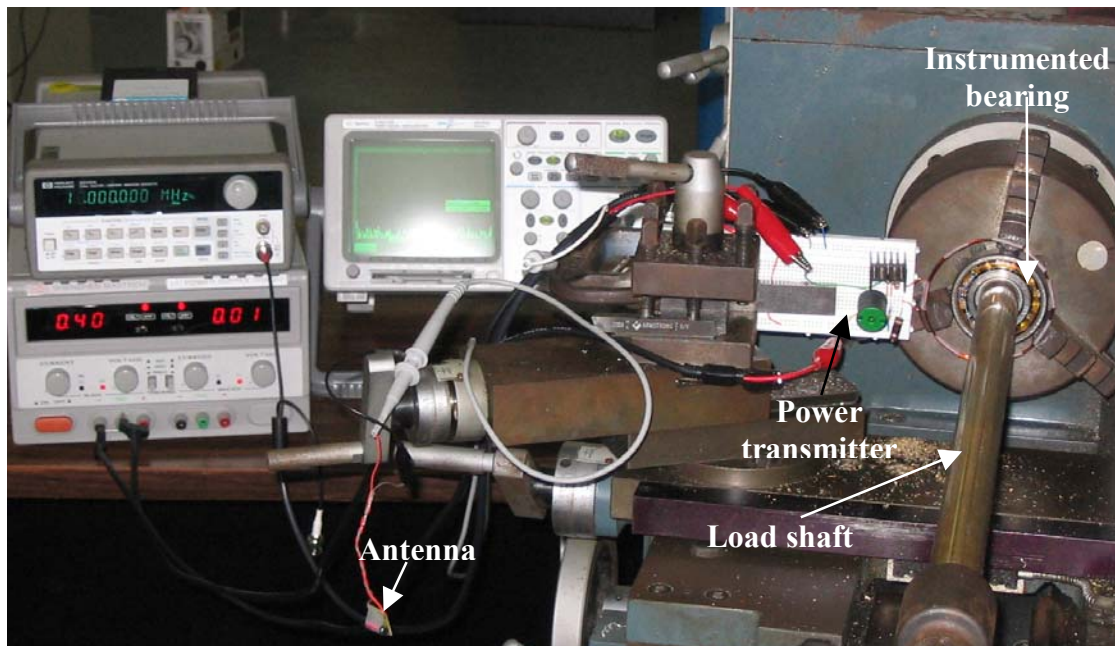


Figure 2. Experimental tests of the RF-powered wireless temperature monitoring system under real operational conditions of a bearing

This work is part of a collaboration between the Electrical and Computer Engineering and the Mechanical Engineering departments in the area of sensor technology for mechanical applications. The integration of sensors in mechanical

components has been a topic of research in recent years. Integrated sensors can be used to monitor the performance of mechanical components and structural health in high-performance applications. This technology can revolutionize monitoring, damage detection, and non-destructive evaluation. Small sensor size, integration into the monitored structure, and the capability to transmit the signal in a convenient fashion are some of the challenges to face in the development of technologies for this type of sensors.

This chapter first overviews the importance of monitoring the temperature in the bearing cage as a useful parameter to determine the condition of the bearing. Next, developments in relevant wireless sensor technologies are reviewed. The chapter ends by presenting the scope and structure of the thesis.

## **1.1 TEMPERATURE IN BEARING CAGE AS A KEY PARAMETER OF CONDITION MONITORING OF BEARINGS**

There is great interest in the development of sensing strategies capable of measuring important parameters of bearings while they are in motion. Rolling element bearings – as basic mechanical components providing support and rotational freedom for rotating machines – have found widespread use in commercial, as well as in aerospace and military applications. Due to their complex design and uneven operation conditions, premature failure of individual bearings can occur. Bearing failure is directly linked to machine downtime, and besides the substantial monetary losses that it can produce, tragic human losses are also possible [1-4]. The development of advanced techniques to monitor the health of bearings while in operation, thus allowing for efficient preventive maintenance and failure prevention, is consequently highly desirable.

Temperature is one of the most important parameters affecting the functional life and performance of rolling element bearings [5-8]. Higher temperatures can affect the bearings in the following ways. A higher temperature results in higher evaporation rates for bearing lubricants which depletes available supply. In addition, higher temperatures

also mean lower lubricant viscosity, resulting in increased wear. Summarizing, elevated and fluctuating temperatures have adverse effects with ultimate bearing failure (see Figure 3).



Figure 3. Thermal overheating results on bearings. Taken from [7].

There are four elements in a rolling bearing: inner and outer raceway, rollers and cage, as shown in Figure 4. The interaction between the rolling elements and the races is based on pure rolling motion while the interaction between the rolling elements and the cage is based on pure sliding motion. Therefore, a greater heat generation is anticipated in the rolling elements and cage contact than that in the rolling elements and inner race or outer race contact. The mass of the cage is smaller than that of the outer race. Also the cage is not in direct contact with any other part of the bearing and as a result the rate of thermal dissipation from the cage is very low. The bearing cage, therefore, will respond faster to an increase in heat input than other bearing component. In addition, the cage guiding the rolling elements is often the starting point of bearing damage [9].

Inner and outer race temperatures are relatively easy to measure. The stationary outer race temperature can be measured directly by using standard devices such as a thermocouple. For the rotating race, slip rings or a commercially available telemetry unit can be added to the shaft in order to transmit the data to a stationary observer.

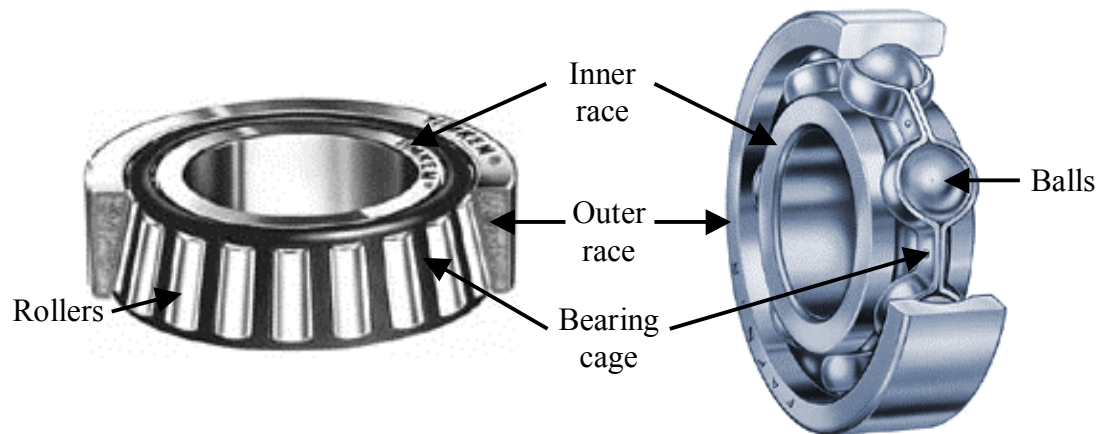


Figure 4. Roller bearing elements. Taken from [10].

Measuring of cage temperatures is significantly more difficult due to the limited space inside bearings, which requires specially designed equipment. Furthermore, the complex motion of the bearing cage prevents the use of slip rings. During bearing operation, the macroscopic motion of the cage is primarily guided by the motion of the rolling elements. However, the microscopic motion of the cage is quite random since the cage is not attached or fixed to any of the bearing component. Currently, there is no way to directly monitor the temperature of the bearing cage. Because a wireless micro-sensor would allow measuring the temperature without wired connections, it can provide an effective solution to this problem.

Several manufacturers (Omni Instruments [11], Microstrain [12] and IR Telemetrics, for example) sell battery powered radio transmitters that can send sensor data from a moving machine component to a stationary receiver. These products are multi-channel, general-purpose designs, often able to handle a variety of sensor types. While some of these products are certainly small enough for many applications, they are too large and heavy for practical use within bearings. Therefore, a smaller, lower-power and robust wireless sensor is needed. The sensor could be powered by a miniature cell battery, however, changing a battery in regular intervals is not practical (or possible) for many applications requiring long-term, unattended operation. Hence, the battery-less operation of these micro-sensors is desirable.

## 1.2 OVERVIEW OF WIRELESS MICRO-SENSORS OPERATED WITH OR WITHOUT BATTERIES

In recent years, the development of methods of wireless signal transmission from remote sensors with or without battery has become an issue of special interest for the design of instrumentation systems. The use of radio telemetry is an attractive option that allows convenient operation in conditions where direct wiring is difficult. Many types of wireless sensing devices have been proposed for different applications such as biomedical implants and monitoring the condition of mechanical parts. These wireless devices typically encode the sensed data, such as pressure, strain and humidity, in the transmission frequency.

Following this recent trend, the feasibility of embedding wireless sensors into functional composite structures is being investigated. Krantz et al [13] developed micro-machined sensors that can be embedded in a composite structure and queried using methods that do not require wired connections. Hautamaki et al [14] used embedded Micro-Electromechanical Systems (MEMS) designed to function as part of a wireless sensing system to measure strain in a composite. The sensing element, signal conditioning, and telemetry circuitry were developed and integrated on a single silicon wafer. However, order-of-magnitude differences between the bulk modulus of silicon and most metals prevent the use of MEMS sensors to measure strain on most mechanical components.

In [15], the authors report the development of an absolute wireless pressure sensor that consists of a capacitive sensor and a planar coil in the same chip. The variable capacitor ( $C_S$ ) and the coil ( $L_S$ ) form a tank circuit whose resonant frequency changes with the applied pressure, as shown in Figure 5. The change in the resonant frequency is remotely sensed by means of an inductive coupling, eliminating the need of wire connections to monitor the pressure. Figure 6 shows the equivalent circuit model for the inductive link used in the telemetric readout system, in which  $L_e$  is the inductance of the

transmitting coil,  $R_e$  and  $R_s$  are the equivalent resistances of the transmitter and sensor respectively and  $M$  is the mutual inductance between the coils  $L_e$  and  $L_s$ . Due to inductive coupling, the external coil stimulates the sensing circuit, and the load impedance is reflected back to the antenna (external coil). By monitoring overall impedance change of the external coil due to the reflected impedance, it is possible to detect the resonance frequency of sensor. This work found that by monitoring the phase of the impedance, the change of capacitance due to the applied pressure was more detectable. Nevertheless, the impedance measured at the external coil requires specialized and expensive instruments. Using the same principle, others authors have developed different versions of wireless capacitive sensors reporting good results [5]. Medical instruments have been manufactured under this principle of operation [16].

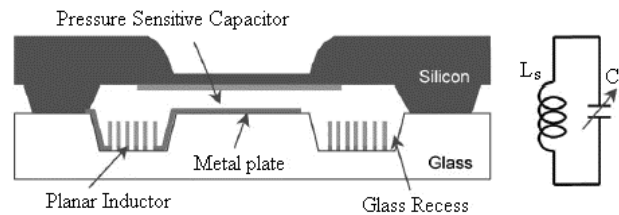


Figure 5. Wireless capacitive sensor and electrical equivalent. Taken from [15].

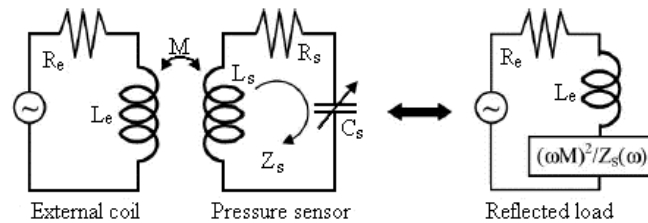


Figure 6. Equivalent circuit model of the wireless pressure sensor. Taken from [15].

A passive wireless integrated humidity sensor was developed in [17]. Here, the concept of reflected impedance in the external coil is used again to detect the variations in a capacitor due to humidity changes. The sensor can be wirelessly monitored up to 1 cm from a stimulating external ferrite core loop antenna. This method of wireless and battery-less sensing is very suitable because it only uses two passive components.

Because of this the use of resistors and active components is avoided and the device can be further miniaturized.

A method to fabricate a sensor skin on a robot was proposed in [18]. The skin contains sensor chips that receive the electrical power and transmit the tactile sensing without wires. Each device is composed of a coil for both sensing and signal transmission, an electrical circuit and a power receiving coil. A sensing coil (stress sensitive) and two capacitances form a Colpitts oscillator. The change of the sensing coil length induces a change in oscillation frequency. The same author in [19] proposed a new wireless tactile sensing device in which the sensing chip is composed of only passive elements. A simple LC resonator (equal to Figure 5) is used: here, the stress sensitive component is the capacitor. The concept of reflected impedance is used for recovering the data by means of an external antenna.

With the objective of precluding the use of batteries in medical implants, inductive powering of these implantable monitoring devices is being more frequently used as a reliable solution [20-22]. Inductive powering is based on the magnetic coupling between two coils, one internal and another external, where the external coil is driven by an AC current. Figure 7 shows the principle of operation of these implants. This system has been widely used in medical applications to supply energy to different monitoring instruments, such as wireless implantable strain monitor of femoral fractures, and intracranial pressure monitor, among others [23].

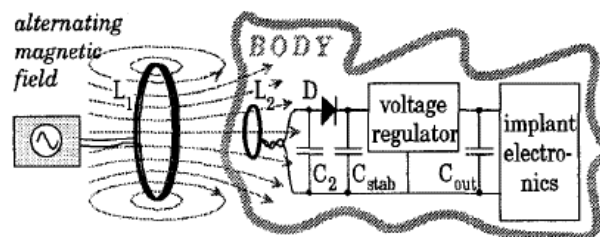


Figure 7. Inductive powering in medical implants. Taken from [21]

A new contact-less technique to provide energy to a micro-system using the capability of a material to generate electric voltage when subjected to a magnetic field (i.e., magneto-electric effect) was developed in [24]. The above magneto-electric effect was implemented by means of a piezoelectric – magnetostrictive laminate. With this technique it is possible to deliver adequate power level for different wireless applications. For bearings, their rotary motion could be used to create a moving magnetic field which induces a voltage into a piezoelectric material or a coil. The magnetic field could be generated by permanent magnets that are attached to a moving part of the bearing (cage, inner race). The coil(s) would be attached to the same part that carries the sensor at stationary part (outer race). This way a direct electrical connection between coils and sensor module is possible. The main advantage of this approach is its ability to generate its own energy. No connections are required; the sensor and telemetry circuits are supplied with energy as soon as the bearing is operating. In regards to the application of measuring the temperature of the bearing cage this method has a disadvantage since the technique requires that the sensing element be static yet the bearing cage will be rotating. Furthermore, high temperatures may have an influence on the magnetization of the permanent magnets.

A method to monitor the operational conditions of rolling element bearings was developed in [6]. Force and temperature sensors and associated electronics were placed in the stationary outer raceway of a ball bearing. Data from sensors was transmitted using wireless communication to a receiver by a frequency-modulated (FM) method. A low frequency was used to send the data; hence the devices were very large. Magnetic coupling between two coils with ferrite core was used as a non-contact method to provide powering, hence, the size of the transducer is increased greatly. With the results of this research, the same authors in [8] proposed an integrated bearing condition monitoring system using a virtual instrument in LabView®.

Many battery-operated wireless sensors applications have been reported in the literature [7] [25] [26]. All of them use the transducer signal to modulate a carrier which

is sent to the receiver using an antenna. Although batteries provide a common source of energy for portable electronics, their applicability to mechanical systems is limited because of their finite useful lifetime as well as the practical difficulties in battery exchange within mechanical environments.

### 1.3 SCOPE AND STRUCTURE OF THE THESIS

The temperature bearing monitoring systems presented in this study consists of a transducer unit, an external data receiver (an antenna), and a central computer (see Figure 8). Temperature sensing elements are placed in an electronic transmitter circuit and located on the bearing cage. Data measured during the bearing operation is wirelessly sent via a modulated carrier signal to an external receiver.

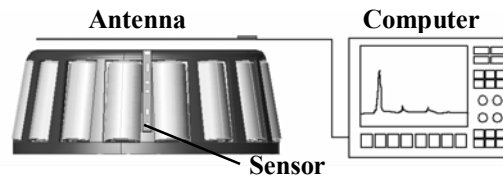


Figure 8. Schematic diagram of the wireless temperature sensor system.

This document is organized as follows. In Chapter 2, the powering techniques used to deliver the energy needed to operate the sensing circuit without the use of direct wires or batteries are described. Chapter 3 presents a study of different methods capable of transmitting wireless data from the sensors to the receiver unit using battery-less circuits. The four data transmission circuits that were designed and implemented in this work are discussed. Chapter 4 shows test results obtained with the sensors described in Chapter 3. Both calibration and results from tests performed in an operating bearing are discussed in Chapter 4. The document ends by summarizing our conclusions and suggestions plans for future work in Chapter 5.

## 2. RF POWER TRANSMISSION FOR WIRELESS SENSORS

One of the main aspects of the present thesis was to find a feasible powering scheme to perform wireless measurements in bearings. While in conventional instruments the main concern associated with power is cost, other considerations are important for applications in which sensors must work in hard-to-reach places and physical access to the sensor is difficult. The simplest power supply, widely used in many portable electronic applications, uses small batteries such as the lithium cells which nowadays are available in the range from 2V, 5mAh, Ø5.8 x 1.2mm to 3V, 540mAh, Ø24.5 x 5mm. Although these batteries are small enough to be placed inside bearings, after some time (i.e. about of 5 hours for the smallest battery if the power consumption of the circuit is 2mW) of continuous operation they must be replaced or recharged. Obviously they do not offer an effective solution for powering devices that must operate during prolonged periods of time inside a bearing. Therefore other powering schemes based on using an external source to deliver energy by means of RF signals were explored in this thesis.

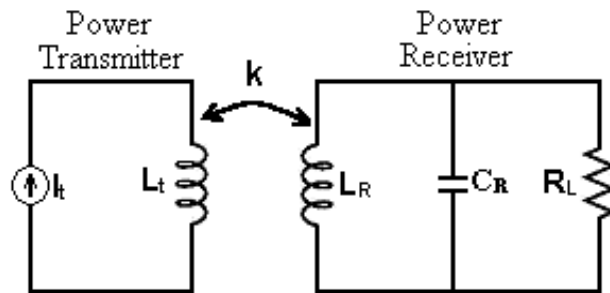


Figure 9. RF powering principle

The main idea of RF powering [27-32] is the use of magnetic energy stored in a transmission coil (primary), as shown in Figure 9. When another coil is placed in the surroundings, a coupling between both coils appears, and by means of electromagnetic induction, a voltage in the receiver coil (secondary) is transferred from the primary coil. Thus this technique uses two coupled coils: the stationary transmitter (primary) which is

connected to a power generator and a secondary which is a part of the portable device, in this case the embedded sensor circuit.

A power system using the RF technique that operates in the 8 - 10 MHz range is described in this chapter.

## 2.1 INDUCTIVE LINK

RF powering [27-33] is based on the magnetic coupling between a transmitter coil driven by an alternating current, and a receiver coil as shown in Figure 9. Both coils form a loosely coupled, coreless transformer (Figure 10). A sinusoidal function generator delivers an AC current ( $I_t$ ) to the primary coil  $L_t$ , inducing a current in the secondary coil  $L_R$ . When the secondary circuit is open, the voltage induced ( $V_{ind}$ ) because of the magnetic coupling is given by equation (1) [37-38].

$$V_{ind} = M \frac{dI_t}{dt} \quad (1)$$

The proportionality constant  $M$  represents the mutual inductance between the two coils [37]. As we can see, the parameter  $M$  determines the received voltage because of the magnetic coupling. Maximizing this parameter helps to have a high-efficiency power link.

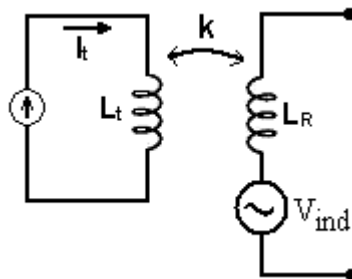


Figure 10. Transformer model for inductive links with a induced voltage ( $V_{ind}$ )

The coupling factor  $k$ , defined by the equation (2), is a useful tool to simplify the analysis of the RF link.

$$k = \frac{M}{\sqrt{L_t L_R}} \quad (2)$$

Here  $L_t$  is the inductance of primary coil and  $L_R$  is the inductance of the secondary coil. The power transferred from the primary into the secondary circuit depends on the coupling factor,  $k$ , which defines the power efficiency of the link.

The inductive coupling problem can be divided into two parts. The first part consists on discovering the mutual inductance between transmitter and receiver antennas. The second half of the problem can be carried out in the circuit domain, and consists on properly designing the link taking into account factors like the excitation frequency and number of turns of the coils, among others. We examine these tasks in order.

### 2.1.1 Mutual inductance

Most inductive links designs employ two circular coils whose turns are concentrated in the circumference of the coil. Hence, calculating the coupling coefficient or the mutual inductance as a function of the ratios of the coil diameters and distance parameters is an important issue in the studies of inductive links. Assuming that the loop conductors can be considered like filaments (see Figure 11), the Neumann's formula (equation (3)) for thin coupled circuits in the free space can be used [37].

$$M = \int_{l_1} \int_{l_2} \frac{\mu_o dl_1 \cdot dl_2}{4\pi R} \quad (3)$$

where  $\mu_o$  is the permeability of free space and  $R$  is defined as in Figure 11,  $l_1$  and  $l_2$  correspond to the filament loops.

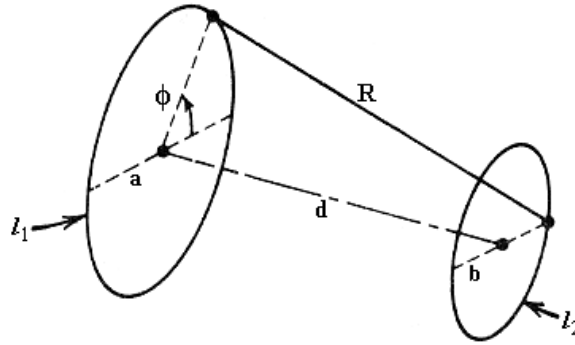


Figure 11. Mutual inductance between two-coaxial filament loops

Using the Neumann's formula and Figure 11, the mutual inductance between coaxial loops [37] can be expressed as

$$M = \mu_0 \sqrt{ab} \left[ \left( \frac{2}{c} - c \right) K(c) - \frac{2}{c} E(c) \right]; \quad c = 2 \sqrt{\frac{ab}{d^2 + (a+b)^2}} \quad (4)$$

where  $a$  is the radius of the primary coil,  $b$  is the radius of the secondary coil,  $d$  is the distance between the two coils,  $\mu_0$  is the permeability of free space,  $K(c)$  and  $E(c)$  are the complete elliptic integrals given by

$$K(c) = \int_0^{\pi/2} \frac{d\theta}{\sqrt{1 - c^2 \sin^2 \theta}} \quad E(c) = \int_0^{\pi/2} \sqrt{1 - c^2 \sin^2 \theta} d\theta \quad (5)$$

Equation (4) refers to single turn coils. In order to calculate the mutual inductance for multi-turn coils, the following approach can be used:

$$M = N_1 N_2 M_{1\text{-turn}} \quad (6)$$

where  $N_1$  and  $N_2$  correspond to the number of turns in primary coil and secondary coil respectively, and  $M_{1\text{-turn}}$  is defined by equation (4).

Another approach [34] to study the mutual inductance of inductive link is as follows. When current passes through the circular loop primary coil, a magnetic field is generated perpendicular to the plane of the loop, given by:

$$B = \frac{\mu_0 I N_1 a^2}{2(a^2 + r^2)^{3/2}} \quad (7)$$

where  $\mu_0$  is the permeability of free space,  $I$  is the current through the primary loop,  $N_1$  is the number of turns in the loop,  $a$  is the radius of the loop, and  $r$  is the distance from the center of the loop along to the loop's axis. The induced voltage in the secondary loop is given by:

$$V = -N_2 \frac{d\Phi}{dt} \quad (8)$$

where  $N_2$  is the number of turns in secondary loop and  $\Phi$  is the total magnetic flux through surface of the secondary loop. The magnetic flux in (8) can be calculated as:

$$\Phi = \int B \cdot dS \quad (9)$$

where  $B$  is the magnetic field given in (7) and  $S$  is the surface area of the secondary coil. Combining (1), (7), (8) and (9) we can obtain the mutual inductance between the coils as:

$$M = \frac{\mu_0 N_1 N_2 a^2 (\pi b^2)}{2(a^2 + r^2)^{3/2}} \quad (10)$$

In this equation,  $b$  represents the radius of the secondary coil. It is important to clarify that the expression shown in equation 10 assumes that the electromagnetic field is essentially uniform over the receiver coil.

Figure 12 shows a comparison between the theoretical values for the mutual inductance between two coils as a function of the coil distance and the secondary coil

radius. These values<sup>1</sup> were obtained from the two model described above in equations (6) and (10). For these simulations, coils with one turn were considered.

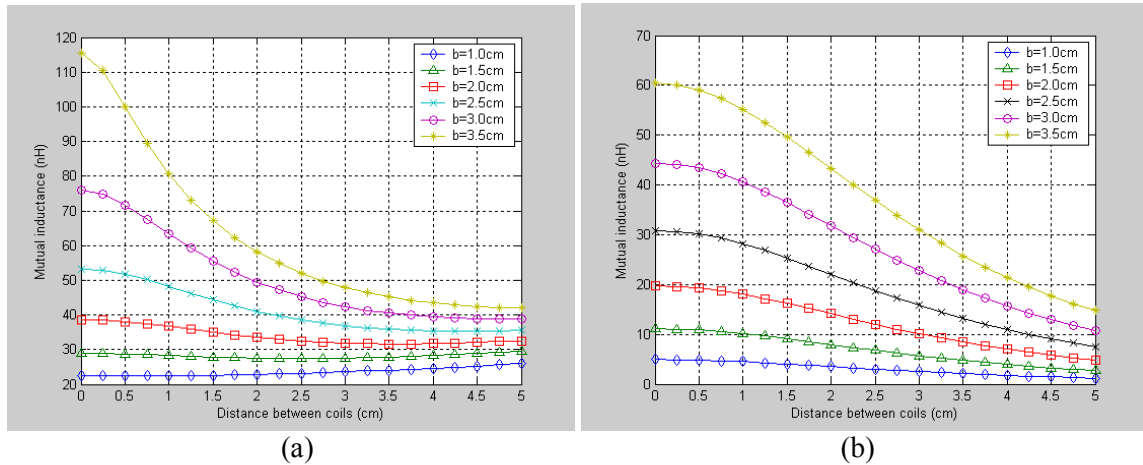


Figure 12. Mutual inductance calculations (a) using model approach of (6) and (b) using model approach of (10)

The results shown in Figure 12 are important because from them we can predict the critical scenarios for the power transfer. The difference between the two models arises from different assumptions in each model. While the model described by equation (6) considers very thin wire loops, the model described by equation (10) assumes that the electromagnetic field is uniform over the secondary (receiver) coil and that the distance between coils is higher than the radius of the transmitter coil ( $r \gg a$ ). However, these models provide a useful tool to select the design parameter of the inductive link.

### 2.1.2 Selecting the frequency of operation

As a general rule, radio signals at lower frequencies will propagate farther than signals at higher frequencies, assuming similar transmitter power levels [38-39]. The attenuation (or decrease) of a radio signal as it travels through a medium such as air is directly related to its wavelength. All signals experience the same decrease in signal

<sup>1</sup> Numerical simulations were done in MATLAB®

strength per wavelength when traveling through the same medium. Because signals at lower frequencies have longer wavelengths, signal attenuation occurs at a slower rate. For example, if signal A decreases by 10% over a distance of 10 feet, then a signal at half of the frequency of signal A will decrease by 10% over a distance of 20 feet, thereby allowing the lower frequency signal to propagate farther. At frequencies less than 100 MHz, other factors have a greater impact on practical communication range. Systems at lower frequencies depend on inductive coupling as the primary mode of interaction [36]. The range of an inductively coupled system drops sharply with distance. Hence, using longer-range electrical coupling at these frequencies is not recommended due to their high susceptibility to noise and interference from other devices.

Previous works in the field of biomedical implants used lower frequency ranges up to 4 MHz [23][28][33]. Radio Frequency Identification (RFID) systems [34-36] use frequencies which can vary from the lower ranges of the spectrum around 135 kHz to the higher ranges at 5.875 GHz. Higher frequencies (more than 100 MHz) are used by battery operated active RFID devices while the most commonly used frequency by passive (battery-less) RFID devices which has a wide range of applications associated with it is the 13.56 MHz ISM (Industrial Scientific Medical) band. Because the operational conditions of bearings do not require a long-range links and to make our approach compatible with actual wireless communication systems such as passive RFID, we decided to use a frequency at 8 – 10 MHz range, which is mainly dominated by the inductive coupling effect.

### **2.1.3 Design and development of inductive link coils**

The mutual inductance analysis described in section 2.1.1 is used as main criterion to design the coils of the system. Optimal coil geometry was obtained from these analyses and then the coils were built and characterized.

According to the mutual inductance analysis, in order to maximize the powering distance of the link, the coil geometry (dimensions) should be increased as much as the application permits. Therefore, the diameter of the receiver coil should be as big as possible. In our case, a diameter of 70 mm was chosen having into account the bearing size. There is a maximum value of mutual inductance as a function of the primary (transmitter) coil radius when the coil distance is small (less than 2 cm) as shown in Figure 13(a). Plots of Figure 13(a) were generated with the mutual inductance model described by equation (6). Using this model, the optimum value of the transmitter coil radius could be in a range from 4 to 4.5 cm. A decreasing behavior of the mutual inductance as a function of the primary (transmitter) coil radius is observed by using the mutual inductance model described by equation (10) and according to the results shown in Figure 13(b), a high mutual impedance is expected if the distance between coils is small and the two coils have similar radius. Taking into account the operational conditions of the bearing, a coil distance in 1 to 2 cm range was established for our application. Similar geometries were chosen for the transmitter and receiver coils to obtain the largest mutual inductance factor possible. Finally, following the above discussion, a value of transmitter coil radius of 4 cm, which according to both models studied in section 2.1.1 will provide greater mutual inductance values (see Figure 13), was chosen.

For both mutual inductance models more turns can be added to the coils to increase the mutual inductance and thus obtain more power transferred. However the size constraints imposed by the application and the finite power of the transmitter limits the use of large inductors.

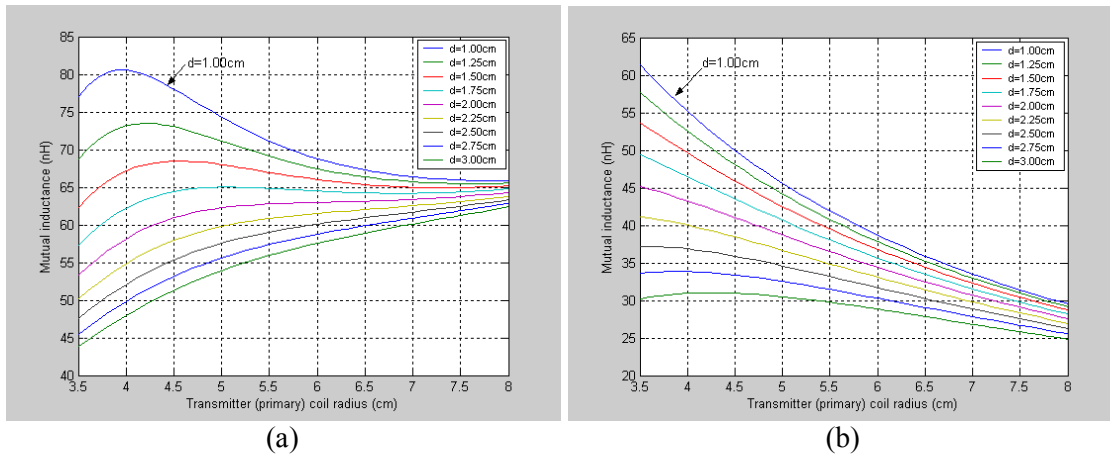


Figure 13. Mutual inductance as a function of transmitter coil radius (a) using model of equation (6) and (b) using model of equation (10). Receiver coil radius  $b=3.5\text{cm}$

Numerous circular geometry loop coils were built and tested during the system implementation. For the wireless system and for the wireless energy transmission tests, the coils showed by Table 1 were used. In Table 1, the inductance of each coil was calculated [37] from,

$$L_{\text{circle}} \cong N^2 \mu_0 R \left[ \ln \left( \frac{8R}{a} \right) - 2 \right] \quad (10)$$

where  $N$  is the number of turns,  $R$  is the radius of the circle,  $a$  is the wire radius and  $\mu_0$  is the permeability of free space.

Table 1. Parameters of inductive link coils

Coil	Wire diameter (mm)	Radius (mm)	Turns	L Calculated $\mu\text{H}$	L Measured $\mu\text{H}$
Transmitter	0.45	40	3	2.066	2.19
Receiver	0.0225	35	1	0.226	0.253

In Table 1, the inductance of each coil was experimentally measured by means of a series RLC resonant circuit which is stimulated with a sinusoidal signal. A frequency sweep of the input signal was done with the objective of finding the resonant frequency

of the circuit. Once this frequency was found and since that the capacitor value was chosen to be fixed, the inductance of the coil was obtained by,

$$L = \frac{1}{\omega_0^2 C} \quad (11)$$

#### 2.1.4 Inductive link circuit model

A circuit model [37] for the inductive coupling between coils is illustrated in Figure 14. The sensing circuit's power consumption can be specified through its minimum power supply voltage and the associated current consumption. Let  $V_o$  represents the voltage induced on the receiver, or sensing, circuit. Applying Kirchoff's Voltage Law (KVL) on loops describes by the currents  $i_p$  and  $i_s$  in the circuit of Figure 14, the equations, in Laplace's domain, that govern the circuit are given by (12) and (13).

$$V_{in}(s) = \left[ R_p + \frac{1}{sC_p} + sL_p \right] I_p - sMI_s \quad (12)$$

$$0 = -sMI_p + \left[ R_s + sL_s + \frac{R_L}{1 + sR_L C_R} \right] \quad (13)$$

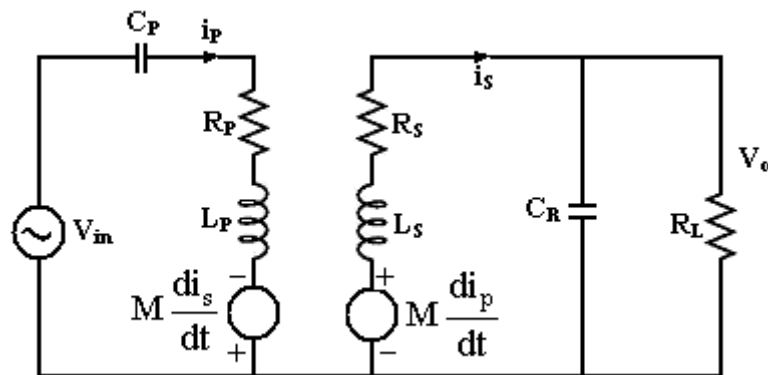


Figure 14. Schematic of the circuit model for the inductive coupling system

If the coils are considered ideal,  $R_p$  only represents the output resistance of the power source ( $V_{in}$ ) and  $R_s = 0$ , from equations (12) and (13) the voltage gain transfer function can be found to be

$$\frac{V_o(s)}{V_{in}(s)} = \frac{M}{L_p} \frac{1}{1 + \frac{R_p L_s}{R_L L_p} + s \left[ \frac{L_s}{R_L} - \frac{R_p}{\omega^2 L_p} - M^2 \right]} \quad (14)$$

Taking into account the parasitic elements of the coils, such as the parasitic primary-coil resistance  $R_p$  (which includes the output resistance of the power source  $V_{in}$ ) and the parasitic secondary-coil resistance  $R_s$ , the voltage gain transfer function becomes

$$\frac{V_o(s)}{V_{in}(s)} = \frac{sM \left( \frac{R_L}{1 + sR_L C_R} \right)}{\left( R_p + \frac{1}{sC_p} + sL_p \right) \left( R_s + sL_s + \frac{R_L}{1 + sR_L C_R} \right) - s^2 M^2} \quad (15)$$

This theoretical calculation allowed us to reduce design time, to obtain a better comprehension of the link, and to get an idea of the relative impact of each variable on the transmitted power. The predictions of the received voltage calculated using (15) with the analytical models for  $M$  described in section 2.1.1 and the experimental results for the voltage received at the secondary coil are compared in Figure 15. For this simulations, the input voltage (in the primary coil) used was 20  $V_{pp}$  at 10 MHz. Equation (6) for  $M$  was used in the model 1, which is very close to the experimental data when the coil distance is very small. Previous works [20-21] in medical implants discuss devices whose operational distances are restricted to operate in these ranges. Equation (10) was used for  $M$  in the model 2, which agrees very well to the experimental data for larger coil distances.

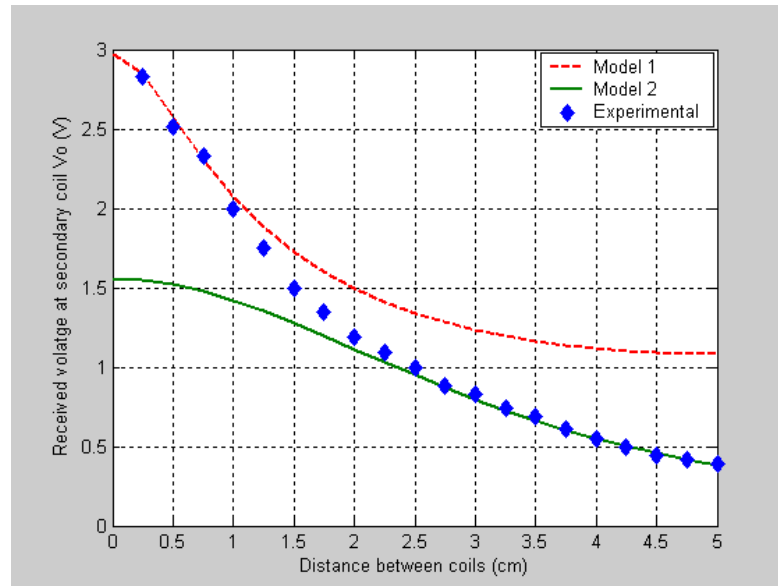


Figure 15. Secondary (receiver) coil voltage vs. coil distance for both models of mutual inductance and experimental data. (Input voltage: 20 V<sub>pp</sub> at 10 MHz)

Some guidelines to maximize the powering distance can be extracted from these results, such as: (1) maximize the mutual inductance by increasing coil geometry (size) as much as the application allows; (2) maximize the induced voltage by increasing the transmitter's voltage, (3) higher frequencies help to obtain higher induced voltages, however, according to simulated and experimental results after 12 MHz, the induced voltage remains almost constant and (4) use a sensing circuit, which is connected to the receiving coil, that can operate at the lowest voltage/power possible.

## 2.2 POWER RECEIVER

This section describes the wireless circuit's power supply. Figure 16 shows schematic diagrams of the energy-receiving circuits implemented in this work. A capacitor is added in parallel with the receiver coil. The reason for this is two-fold. First, as the resonant capacitor cancels the impedance of the secondary coil, the load "seen" by the primary is purely resistive. Second, using parallel resonance helps to achieve a better coupling efficiency [21] [27].

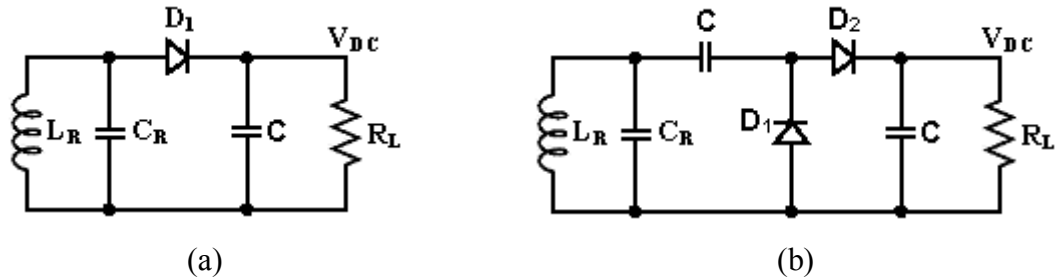


Figure 16. Energy receiver circuits. (a) Half bridge configuration and (b) voltage doubler configuration

Depending on the coupling factor of the link -which varies mainly with the distance- a certain voltage signal is induced (see section 2.1.1). Amplitude ranges can go up to  $20 V_{pp}$  if strong coupling and a very efficient transmitter are used. The RF signal induced across the receiver coil  $L_R$  is rectified in further stages to provide a DC voltage to the rest of the sensing circuit. In case this dc signal is very large, a regulation stage could be added.

## 2.2.1 Component selection

### 2.2.1.1 LC tank receiver

The value of capacitor  $C_R$  was chosen so that the resonant frequency of tank circuit ( $L_R C_R$ ) receiver matched the transmitter frequency. The capacitor value was chosen taking into account that the frequency range of the RF powering was selected to be between 8 and 10 MHz, and given the inductor value discussed in section 2.1.3. Since the application requires small size, surface mount (SMT) components were used for the capacitor. Hand-made air coils (see section 2.1.3) and commercially available capacitors were used to match the specified frequency. For the chosen operating frequency of 10 MHz, the inductance of the power receiving coil and the capacitor that resonates with this coil value were selected according to Table 1 to be 226 nH and 1000 pF, respectively.

### **2.2.1.2 Rectifier circuit**

The power supply rectifier must be designed with care because a bad selection of its components may result in very high power losses due to large voltage drop across the diode. High frequency rectifiers have two loss contributions associated with the diodes [27] [40], due to its forward conduction and to the component's finite switching time, respectively.

The switching losses occur as a consequence of the reverse recovery time of the diode. However, they can be eliminated using Schottky diodes. Tests done using high-speed conventional diodes show a very poor switching time, and therefore Schottky diodes were used for the rectifier circuit

The diode's voltage drop has two components due to the pn-junction and the non-zero parasitic series resistance, respectively. Since the weak coupling factor of most inductive links makes it difficult to induce a high secondary voltage, half-wave rectifiers are often preferred over their full wave counterparts because they reduce the number of diode voltage drops (see Figure 16). A voltage doubler configuration can be used if the sensing circuit operation requires a higher voltage. In this work, a half-wave rectifier was implemented for the device developed in section 3.1, a voltage doubler configuration was used in the sensor of section 3.2 and a full-wave rectifier was used in the sensor developed as in section 3.4.

## **2.3 POWER TRANSMITTER**

The main task was to design and implement a RF transmitter able to give enough power to the sensing circuits. The only practical solution to supplying sufficient power to the receiver is to generate a large primary current in the transmitter coil. The circuit to drive the primary coil is thus a very important element of the transmitter. This section explains several transmitters for driving inductive links and the reasons for which the

class-E transmitter amplifier was selected as the best choice. Design methods and issues for Class-E power amplifier are then described.

### **2.3.1 Driver circuits for inductive links**

There are many types of drivers that can be used to this application, mainly conventional switch-mode resonant drivers. The choice of a transmitter which drives the inductive link depends on how the transmitter coil is tuned and how much efficiency is required. The embedded receiver resonant circuit (see section 2.2.1.1) is usually parallel tuned. The transmitter resonant circuit can either be series or parallel tuned [42]. A series-tuned circuit requires a voltage source for driving such as a class-D or class-E amplifiers. A parallel resonant circuit requires a current source to drive it, e.g. a class-C power amplifier. Switch-mode amplifiers, in general, permit an efficient DC-to-AC conversion at radio frequencies in resistive loads. Class-C amplifiers have limited efficiency in the 60 – 70% range. This is rather low when compared to class-D and class-E amplifiers, which have efficiencies in the 80 - 100% range. High efficiency is desirable for stand-alone applications.

As mentioned before, class-D and class-E amplifiers can drive series-tuned circuits. A class-D amplifier uses two active devices to switch the input of the tuned circuit between the two power supplies [43]. This driver is highly efficient, but suffers from the possibility of both active devices (e.g. transistors) to conduct simultaneously or to be off simultaneously during the switching transient, which would lead to a loss of efficiency at high frequencies, and even device destruction [44]. Finally, these amplifiers require complex drive circuits.

Because of the problems related with class-C power amplifiers and as class-D power amplifiers need two active devices to properly operate, the class E amplifier is a more suitable choice for driving the coil transmitters for our wireless powering sensor

application. Previous works in this area employ this type of driver for medical implants [27-30].

### 2.3.2 Class-E power amplifier design

Sokal and Sokal in [44] presented the class-E amplifier for the first time in 1975. Since then, this configuration has been studied and surveyed by numerous researchers [45-49]. A simple example of a class-E tuned power amplifier is shown in Figure 17. A class-E power amplifier consists of a transistor (which can be a BJT or a FET) with a parallel capacitor  $C_1$ , an RF choke inductor ( $L_{\text{choke}}$ ) and a series RLC load network. In this configuration, the inductance  $L_t$  of the RLC load network was used as the transmitting coil in the powering system.

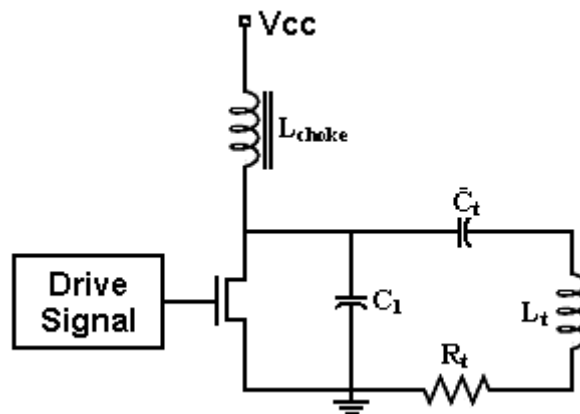


Figure 17. Simple class-E tuned power amplifier

The transistor is operated as an ON/OFF switch at the operating transmission frequency. The RF choke is assumed to act as a DC-current source and exhibits large impedance at operating frequency. The capacitor in parallel with the transistor, which also includes the parasitic output capacitance of the transistor, prevents immediate voltage changes at the drain/collector of the transistor.

To simplify the analysis, we consider the transistor as an ideal switch, which is a short circuit when ON, an open circuit when OFF, and can switch between the two states

instantaneously. In the OFF state, DC-power is delivered to the series-tuned circuit ( $L_t$ ,  $C_t \parallel C_1$ ,  $R_t$ ). The load current  $i(t)$  is determined by the resonance properties of circuit ( $L_t$ ,  $C_t \parallel C_1$ ,  $R_t$ ). In ON state, the voltage across  $C_1$  is zero. Thus current  $i(t)$  depends only on the properties of circuit ( $L_t$ ,  $C_t$ ,  $R_t$ ); and the influence of  $C_1$  is eliminated. For an ideal switch, the voltage across  $C_1$  is zero when the switch is ON and therefore the power dissipated by the transistor is zero, so the theoretical efficiency of this ideal class-E amplifier is 100%.

Different design procedures for class-E amplifiers have been discussed in the literature [44-49], each one makes different assumptions and design considerations. These studies show that optimum operating point and power output capability are obtained when the duty cycle  $D$  of the input signal to the driver is 50% ( $D=0.5$ ). However, this is not a restriction for proper class-E tuned amplifier design. In fact, highest output power to a given load occurs when the duty cycle is less than 0.5, at the expense of reduction in efficiency [43].

An analysis of the class-E amplifier was done by Raab in [45]. As a result of this, a set of equations for a 50% duty cycle of the switch operation were given. A detailed analysis is described by Kazimierczuk and Puczek in [46] in which the design of class-E amplifiers for different switch duty cycles is shown. For our design, signals with duty cycle of 50% were considered.

The explicit design equations for the choice of  $D = 50\%$  are given by [45][49]. In the equations below,  $V_{CC}$  is the DC-supply voltage.  $P$  is the output power delivered to the load resistance  $R_t$ ;  $f$  is the operating frequency;  $C_1$ ,  $C_t$ ,  $L_t$  and  $L_{choke}$  are the load network shown in Figure 17.  $Q_L$  is the network loaded  $Q$ , chosen by the designer. The design procedure as follows:

$$V_{CC} = \frac{V_{DS,peak}}{3.56} \quad (16)$$

The relationship among  $P$ ,  $R_t$ ,  $Q_L$ ,  $V_{CC}$  and the transistor saturation voltage  $V_{sat}$  has been widely studied. Kazimierczuk and Puczek in [46] give this relationship in a tabulated form over a wide range of  $Q_L$ . From an approximate expression for  $P$  given by equation (17), the value of  $R_t$  can be found by equation (18).

$$P = \left( \frac{(V_{CC} - V_{sat})^2}{R_t} \right) \left( \frac{2}{\frac{\pi^2}{4} + 1} \right) \cong 0.576801 \left( \frac{(V_{CC} - V_{sat})^2}{R_t} \right) \quad (17)$$

Hence:

$$R_t = 0.576801 \cdot \left( \frac{(V_{CC} - V_{sat})^2}{P} \right) \quad (18)$$

The design equations for  $C_1$  and  $C_t$  are found using the tables of Kazimierczuk and Puczek in [46]. Using the coil design obtained in section 2.1.3, with a resultant transmitting coil of 2.19  $\mu\text{H}$  and a frequency operation of 10 MHz according to section 2.1.2, and following the Kazimierczuk equations and from the desired values for  $V_{CC}$  and the voltage across the load, Table 2 was generated. According to these design parameters a quality factor  $Q_L$  of 14 was chosen. The choke inductance should guarantee that the supply current of the amplifier remains approximately constant during the RF cycle, however, is not a limiting factor. A relationship commonly used is

$$X_{L\text{choke}} > 30 \frac{1}{2\pi f C_1} \quad (19)$$

Table 2. Design components of class-E power amplifier

$Q_L$	$R_t$ ( $\Omega$ )	$C_1$ (nF)	$L_t$ ( $\mu$ H)	$C_t$ (nF)	Resonance frequency (Hz)
2	10.09	0.3481	0.32	4.914	4,005,328.88
3	10.09	0.3436	0.48	1.007	7,224,848.86
4	10.09	0.3364	0.64	0.592	8,160,110.26
5	10.09	0.3299	0.80	0.424	8,620,791.14
6	10.09	0.3246	0.96	0.332	8,896,267.26
7	10.09	0.3204	1.12	0.273	9,079,787.60
8	10.09	0.3171	1.29	0.232	9,210,885.66
9	10.09	0.3143	1.45	0.202	9,309,243.81
10	10.09	0.3120	1.61	0.179	9,385,777.10
14	10.09	0.3059	2.25	0.123	9,574,339.68
20	10.09	0.3011	3.21	0.084	9,708,515.99

The choice of the switching active device is another important design consideration. As mentioned before this device can be a BJT or FET transistor. The transistor should have a maximum drain-to-source voltage at least 3.6 times larger than the supply voltage used. Since the driver needs the capacitor shunt for proper operation, the output capacitance of the transistor is not a limiting factor. The device used in this application is a power N-channel MOSFET IRF510N, which has a maximum drain-to-source voltage of 100V, maximum power dissipation of 43 W and parasitic output capacitance of 80 pF.

### 2.3.3 Results

Overall efficiency  $\eta$  of an RF-power transmitter is defined as the ratio of the power delivered to the load (sensing circuit) and the overall DC-power consumed by the whole system. Efficiencies (DC – to – AC conversion) above 60% were measured in the class-E amplifier. Table 3 shows the results obtained for the overall power efficiency. These results were obtained for a class-E power transmitter operating at 10 MHz; the measurements were taken at a fixed distance of 2.5 cm and with a 1K $\Omega$  load, simulating the sensing circuit consumption. From the results, overall efficiencies of power transmission in the range of 14% were obtained.

Table 3. Power efficiency of the system

$V_{CC}$ (V)	$I_{CC}$ (mA)	$V_{Load @ 1 k\Omega}$ (V)	Load power (W)	Overall efficiency
5	78	7.70	0.0593	15.2 %
7	106	10.25	0.1051	14.2 %
9	130	12.7	0.1545	13.2 %

A simple test was performed to measure the effect of distance between coils on the received power. The DC voltage in a  $1k\Omega$  resistance was measured while the distance between the coils was changed. Figure 18 illustrates the experimental setup. The results obtained from this test are shown in Figure 19. According to these results, power levels in the 16 to 100 mW range were obtained. A load power level of approximately 16 mW was obtained for inter-coil distances of up to 6 cm. This amount of power is sufficient to energize our sensing circuit. For closer distances larger DC-power levels can be reached up to about 100 mW. Therefore, enough power for our application could be transmitted for distances of up to 6 cm. between the power transmission and reception coils. The performance obtained from this system is thus appropriate for our application.

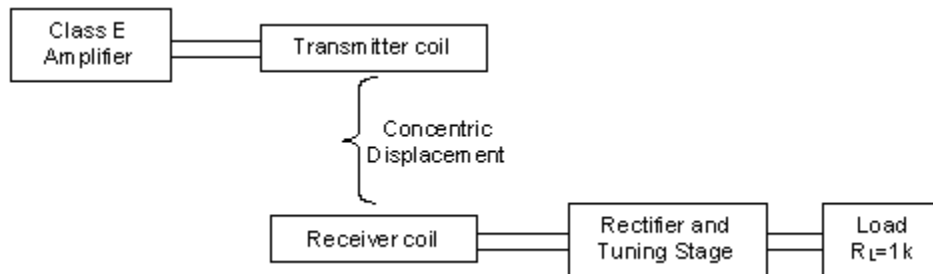


Figure 18. Setup used to measure the received DC voltage as a function of the distance between the coils.

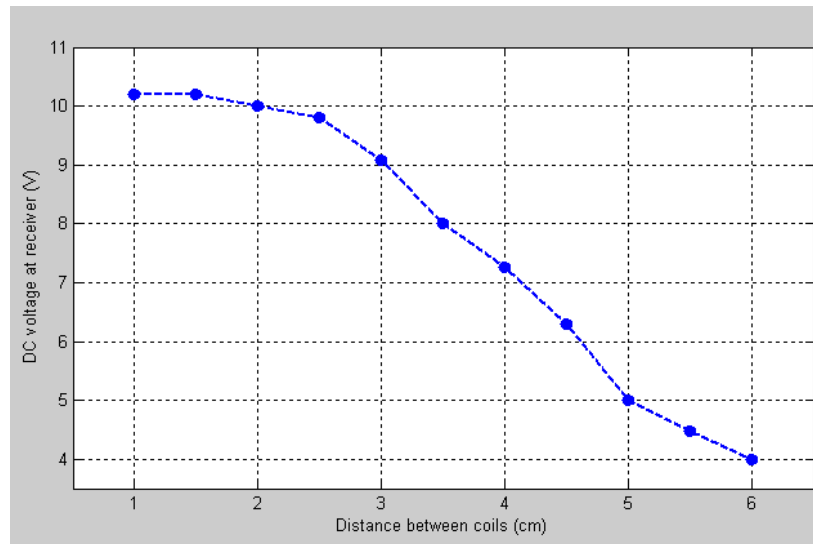


Figure 19: DC Voltage at receiver circuit as a function of the distance between coils

## 2.4 SUMMARY

Experimental results show that the powering of wireless sensor systems can be done by using an RF inductive link which employs a high efficient class-E power amplifier. Theoretical models were used to optimize the inductive link design and to reduce the time employed in the design. From this theoretical effort, several design considerations for the inductive link were extracted in order to maximize the powering distance of the receiver circuit such as: maximize mutual inductance by maximizing coil geometry, maximize the primary coil current by increasing the transmitter voltage, use low power and low voltage operated circuit at receiver.

Using these theoretical considerations, an RF powering circuit of proper performance was designed and developed for our application. The small size requirement can be obtained by means of the use of SMT devices in the sensor's circuit.

### 3. TEMPERATURE WIRELESS SENSING CIRCUITS

This chapter presents the development of four wireless systems for bearing cage temperature measurements without using batteries as an energy source. Each wireless system is labeled according to its operational principle: LC Colpitts oscillator, Voltage Controlled Oscillator (VCO), Meissner Oscillator and RFID. The RF powering technique discussed in the Chapter 2 was used to energize the sensing and wireless transmission data circuits. The chapter ends with a description of the fabrication of the wireless sensors developed and its installation procedure on roller and ball bearings.

#### 3.1 COLPITTS OSCILLATOR – BASED TEMPERATURE SENSOR

##### 3.1.1 Principle of operation

This RF-powered system employs a frequency-modulated (FM) RF signal to transmit data wirelessly. The circuit, shown in Figure 20, is an inductor-capacitor (L-C) tuned oscillator. The transmission coil L and the sensing capacitance  $C_1$  and  $C_2$  form an oscillator [51-52] with resonance frequency given by,

$$\omega = \frac{1}{\sqrt{LC_s}}, \quad \text{Where:} \quad C_s = \frac{C_1 C_2}{C_1 + C_2} \quad (20)$$

Temperature sensitive capacitors ( $C_1$  and  $C_2$ ) mounted on a bearing cage are integrated into the L-C oscillator as frequency-controlling elements. The change in capacitance due to temperature variation translates into modulation of the oscillator frequency. An advantage of this type of circuits is that the frequency of the Colpitts oscillator does not depend on the voltage supplied to the circuit. Thus, fluctuations in the DC voltage generated by means of the RF powering technique described in Chapter 2 do not have a great effect on the temperature readings.

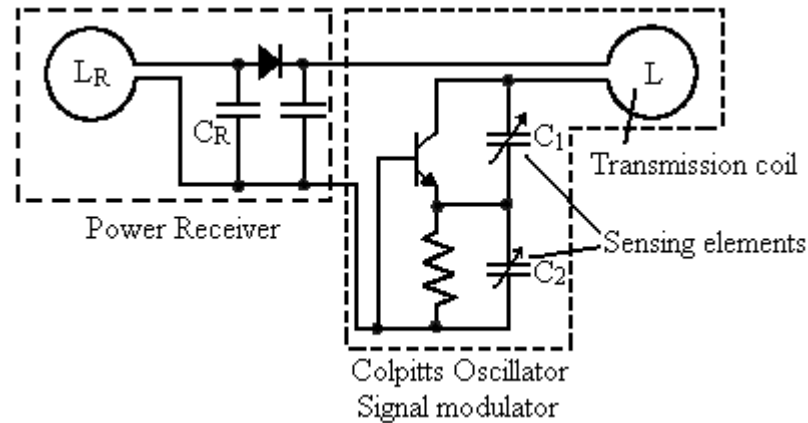


Figure 20. Schematic for RF-powered wireless temperature sensor based on Colpitts oscillator.

Commercial capacitors vary somewhat with changing temperature. Most capacitors have a negative temperature coefficient. However, the temperature coefficient (change in capacitance vs. change in temperature) is not always linear. Capacitors with temperature-sensitive dielectric are available from several manufacturers. Here is some information about the temperature characteristics of some common dielectric types of capacitors [53-54]:

- **COG or NPO** (negative-positive zero) capacitors are the most stable with temperature; they have a temperature coefficient that is ideally zero.
- **X7R** capacitors have a non-linear temperature characteristic which exhibits a dielectric constant variation of less than  $\pm 15\%$  from its room temperature value, over the temperature range from  $-55^{\circ}\text{C}$  to  $125^{\circ}\text{C}$ .
- **Y5V** capacitors give the largest values in the smallest size package. The temperature coefficient is terrible, often falling to  $-80\%$  from its room temperature value when it is submitted at  $+85^{\circ}\text{C}$ .

The behavior of the capacitance change due to the temperature for capacitors with dielectric types X7R and Y5V are shown in Figure 21. Using an appropriate combination of capacitors in  $C_1$  and  $C_2$  yields a detectable change in the frequency of the oscillator

(19). The use of a negative temperature coefficient in both capacitors helps to increase the resolution of the temperature measurement because the capacitance changes in each element have a multiplier effect on  $C_S$  in equation (20). The range of operation is determined by the portion of the curve in which the capacitance change due to temperature is approximately linear. For this case, as seen on Figure 21, the possible operational range is from 20°C to 80°C. This temperature range agrees well with the values exhibited by bearings during working conditions [1][3][6-7]. Hence, these types of capacitors were used in this project.

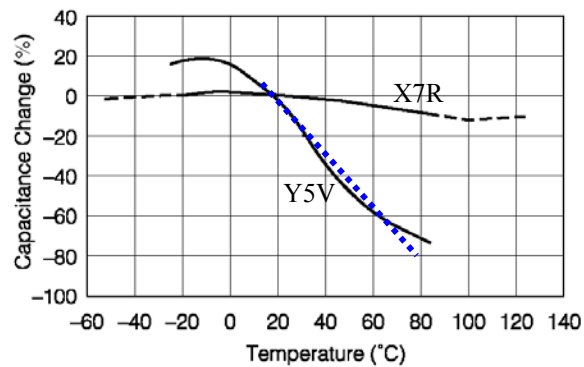


Figure 21. Temperature behavior for X7R and Y5V dielectric type capacitors. Taken from [53-54]

### 3.1.2 Circuit design

The system proposed has two carrier frequencies: one was used to receive the power and the other to transmit the temperature data. As the carrier frequency of the power signal was chosen to be 10 MHz according to the section 2.1.2, then the carrier frequency of the temperature data was chosen to be in the 1 to 2 MHz range. These frequency ranges are far enough to allow detection of the frequency-modulated signal that contains the temperature data.

The design of the Colpitts oscillator was done using an Y5V dielectric type capacitor for  $C_1$  and a X7R dielectric type capacitor for  $C_2$ . As mentioned before, the temperature/capacitance-change for this combination is nearly linear over the operating

range of 20°C to 80°C (Figure 21). The negative temperature coefficient of both capacitors helps to increase the resolution of the measurement.

The design problem consists on determining the component values using the circuit shown in Figure 22 (a) for the selected operating frequency. A small signal analysis of the Colpitts oscillator circuit yield design criteria for selecting  $C_1$ ,  $C_2$  and  $L$ . The values for these components must be chosen so that the Barkhausen conditions are satisfied [52]. From analysis of the equivalent circuit shown in Figure 22 (b), the feedback network's  $\beta$  is

$$\beta = \frac{C_1}{C_1 + C_2} = \frac{C_S}{C_2} \quad (21)$$

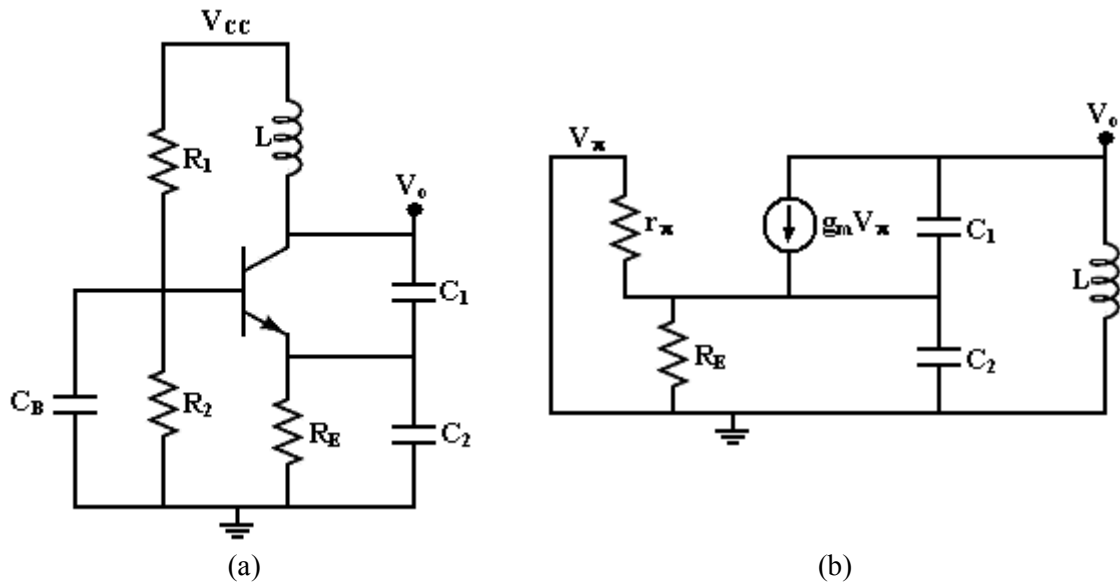


Figure 22. Colpitts oscillator diagram for component selection. (a) DC analysis and (b) AC analysis.

The open loop gain operation of the amplifier ( $A_V$ ) is restricted so that

$$A_V \geq \frac{C_2}{C_S} \quad (22)$$

As the effective resistance of the inductance  $L$ ,  $R_L$ , is related to the open loop gain,  $A_V$ , another design condition for the resistance value of  $L$  is given by (23).

$$R_L \geq \frac{r_\pi}{\beta \cdot h_{fe}} \quad (23)$$

To obtain stable oscillations the quality factor  $Q$  of the resonant circuit needs to be as high as possible. The  $Q$  is usually determined by the inductor. The inductance value of the oscillator circuit must be chosen having in account these last two design issues: resistance and quality factor. From the value of the operational frequency and assuming an inductance value for  $L$ , the value of the sensing capacitance was found using (24).

$$C_S = \frac{1}{\omega^2 L} \quad (24)$$

The other components of the oscillator circuit,  $R_1$ ,  $R_2$ ,  $C_B$  and  $R_E$  are biasing components and were chosen from a DC analysis of the circuit to obtain an emitter current of 1mA with a DC supply voltage of 2.5V.

Figure 23 shows the RF-powered wireless temperature sensor developed in the present project.

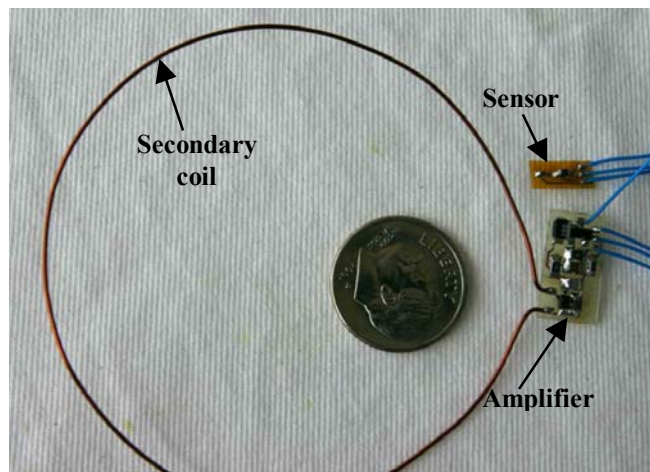


Figure 23. RF powered wireless temperature sensor using a Colpitts Oscillator

With the objective of increasing the capture range of temperature data, the oscillation frequency was increased. Since implementation with a single oscillator was not possible because it would have required component values that were not feasible, an approach using two Colpitts oscillators was done, as shown in Figure 24. The temperature sensitive capacitors establish the frequency of the first oscillator in the 1 kHz to 10 kHz range. The output of this stage is coupled to the second oscillator which is used to modulate the data in an 88 MHz to 108 MHz range. The modulated signal is received by a commercial FM receptor which is in charge of demodulating and recovering the temperature information.

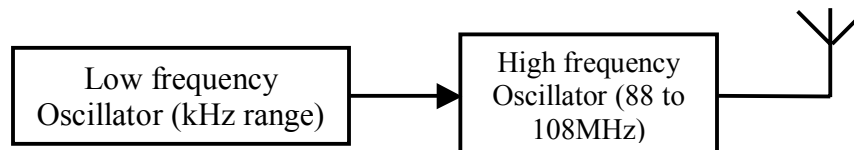


Figure 24. Block diagram for a wireless temperature system using two Colpitts oscillators.

Figure 25 shows the power spectrum of two signals received using the approach described above. Each power spectrum shows a main frequency component and several harmonics of this fundamental frequency. The capture range for this circuit was very good, up to 1 m. However, the circuit was not used in other experiments because the large number of components precludes its use inside a bearing.

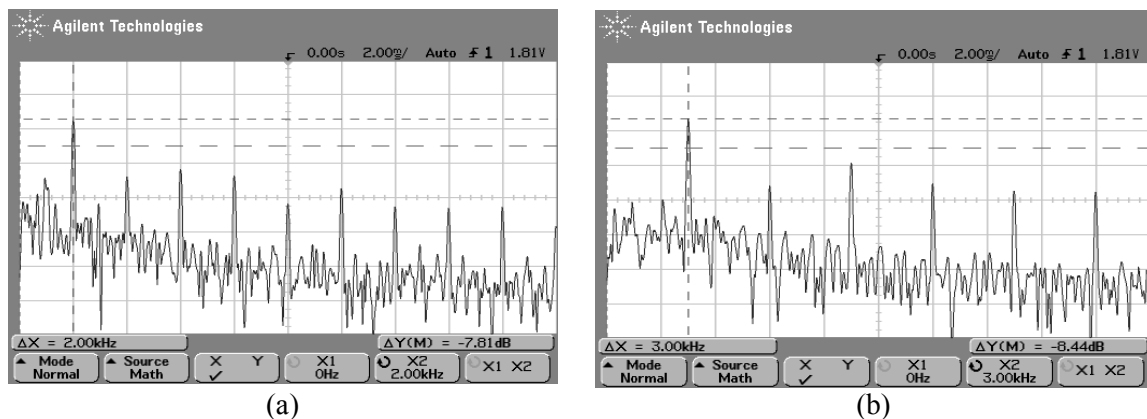


Figure 25. Power spectrum of a received signal using two Colpitts oscillators configuration

## 3.2 VOLTAGE CONTROLLED OSCILLATOR – BASED TEMPERATURE SENSOR

### 3.2.1 Principle of operation

This section explores the possibility of using an integrated oscillator to transmit the temperature data. The carrier frequency used in this approach is higher than the one used in the Colpitts oscillator described in section 3.1. The circuit uses an off-the-shelf integrated Voltage Controlled Oscillator (VCO) which is widely used in modern wireless systems. A VCO [56-57] is an oscillator whose frequency can be varied by an input voltage. Because of this, the sensing element must output a voltage as a function of the temperature data. Integrated-Circuit (IC) temperature sensors were used in this system because of its very small size, very low power consumption and very high linearity.

National Semiconductors' LM60 [55] is a 3-terminals precision IC temperature sensor that can sense a  $-40^{\circ}\text{C}$  to  $+125^{\circ}\text{C}$  temperature range while operating from a single  $+2.7\text{V}$  supply (see Figure 26). The LM60's output voltage is linearly proportional to temperature with a proportionality constant of  $+6.25\text{mV}/^{\circ}\text{C}$  and has a DC offset of  $+424\text{mV}$ . Table 4 shows the typical output voltages for the whole temperature range of the sensor. The offset allows reading negative temperatures without the need for a negative supply. The IC-temperature sensor (LM60) mounted directly on the bearing cage was used as a frequency-controlling element for an integrated VCO.

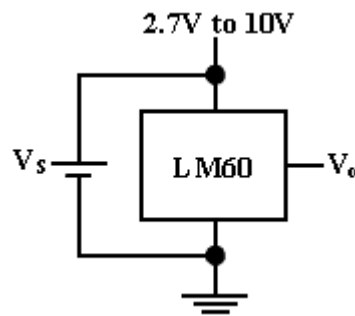


Figure 26. Connection diagram for LM60 IC-temperature sensor

The most common means for electronically tuning an oscillator is with a varicap or varactor diode [58]. This diode is operated with a reverse bias on the junction. So, the capacitance is a function of this reverse bias. A typical VCO uses a varactor as a tuning element within a Colpitts topology, as shown in Figure 27.

Table 4. Full-range Centigrade temperature of LM60 IC-temperature sensor

Temperature	Typical $V_o$
+125°C	+1205 mV
+100°C	+1049 mV
+25°C	+580 mV
0°C	+424 mV
-25°C	+268 mV
-40°C	+174 mV

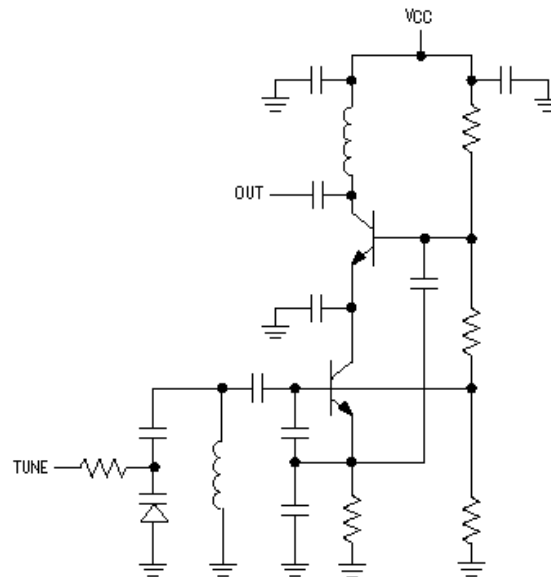


Figure 27. VCO implemented with discrete circuit elements. Taken from [57]

### 3.2.2 Circuit design

In a conventional VCO design [56-58], the oscillator core and the output amplifier stage can be built using discrete transistors, resistors, capacitors, and inductors as was shown in Figure 27. The tank is built from a network consisting of the frequency-setting

inductor, varactors, coupling capacitors, and feedback capacitors. The output stage uses reactive elements to match the output impedance of the circuit with a specified load network.

To ensure a successful design, the component values not only must establish a desired nominal oscillation frequency, but they must also guarantee an adequate tuning range, proper biasing, oscillator startup under all conditions, and proper output-stage performance. Problems can occur even with a good first-order design because of the trade-off that exists among current consumption, startup margin, frequency tuning range, and phase noise. A major disadvantage of discrete VCO designs is the amount of Printed Circuit Board (PCB) area required. The layout contains parasitic capacitances and inductances that affect the oscillation frequency and must therefore be taken into account to implement the oscillator properly.

The integrated VCO family from MAXIM [56-57] offers a better alternative than a discrete VCO. These ICs (MAX2605-MAX2609) are designed for low-power and portable wireless applications with frequencies in the 45MHz to 650MHz range. The varactor and feedback capacitors are integrated on-chip so that only an external inductor is required to establish the frequency of oscillation and produce a properly operating VCO. The tuning range, biasing, startup, etc., are all managed within the IC, eliminating the design headaches typically associated with the VCO design. Furthermore, this IC presents size advantages because of its tiny package (Figure 28).

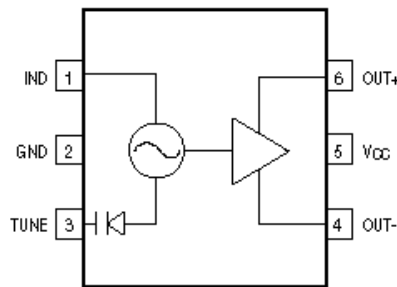


Figure 28. Integrated VCO from MAXIM. Taken from [57]

To select the oscillation frequency of the VCO, an adequate value of the inductance at IND pin of the chip must be chosen. An inductance versus oscillation frequency plot in the product datasheet [59] simplifies the task of choosing this external inductor. According to the manufacturer the input voltage at the TUNE pin of the chip (control voltage of the VCO) must to be in the 0.4 V to 2.4 V range, hence, this range establishes the frequency limits of the VCO as well. The output voltage range of the IC-temperature sensor (see Table 4) for the temperature range of the bearing operation (25°C to 80°C) is within the constraint voltage values imposed by the manufacturer of the chip.

Figure 29 shows the schematic diagram of the circuit used for the RF powered wireless temperature sensor based on a VCO. As we have said, the input voltage ( $V_{\text{control}}$ ) is the output voltage of the IC temperature sensor. The system proposed has two carrier frequencies as in the Colpitts principle, one to receive the power and other to transmit the temperature data.

Because carrier frequency of the power signal was chosen to be 10 MHz, then the carrier frequency of the temperature data was chosen to be in the 50 MHz to 60 MHz range. The inductor  $L_f$  was chosen to set this oscillation frequency range for the VCO.

The integrated VCO has a differential amplifier as the output stage. This output can be used in a single ended form or a differential form. However, a higher output power can be reached by using the differential mode. The outputs (OUT+ and OUT-) are open-collector type and hence they require pull-up elements to  $V_{CC}$  to operate properly.  $R_1$  and  $R_2$  in the Figure 30 are 1 k $\Omega$  pull-up resistances which supply a DC bias for the output stage. The 1 k $\Omega$  value is used to maximize the swing to the load. Figure 30 shows the RF-powered wireless temperature sensor based on a VCO principle developed in the present project.

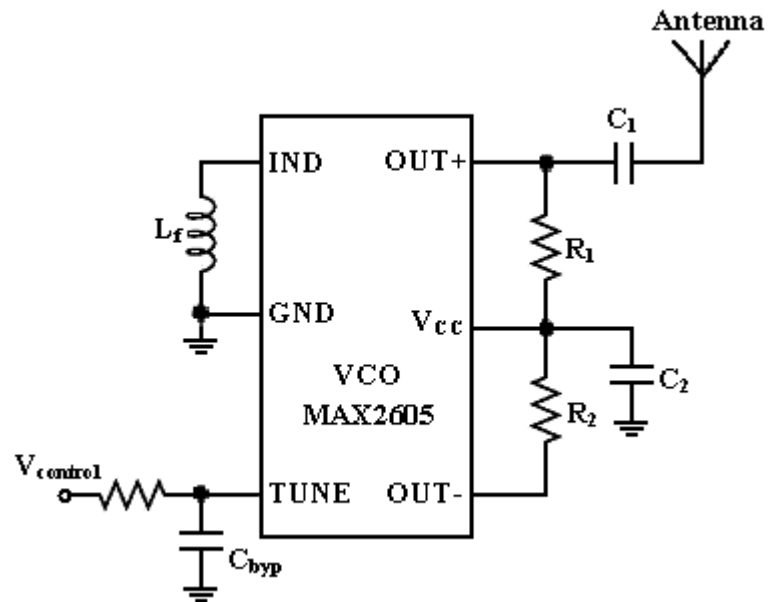


Figure 29. Schematic diagram for RF-powered wireless temperature sensor based on a Voltage Controlled Oscillator.

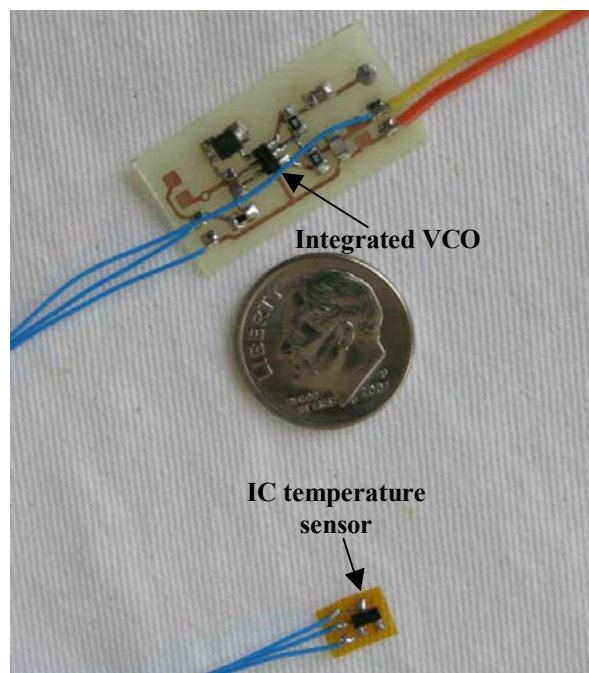


Figure 30. RF powered wireless temperature sensor using a Voltage Controlled Oscillator and an IC temperature sensor

### 3.3 MEISSNER OSCILLATOR – BASED TEMPERATURE SENSOR

#### 3.3.1 Principle of operation

This wireless sensor contains only two-components in the remote circuit and uses the Meissner oscillator principle [60]. While in the RF-powered wireless temperature sensors presented in sections 3.1 and 3.2 the whole sensing circuit (power receiver + oscillator + transducer) must to be installed over the bearing, in this approach only two-components (a coil and a temperature-sensitive capacitor) were located on the rotating part.

Figure 31 shows the schematic diagram for the Meissner oscillator. The sensor unit is a simple resonator with two-components: the capacitive transducer (C) and a coil (L). The coil in the sensing resonator is magnetically coupled with an amplifier by means of two coils but there is no contact between them. The natural frequency of the resonator determines the frequency of the Meissner oscillator given by (25).

$$\omega = \frac{1}{\sqrt{LC}} \quad (25)$$

The capacitance changes in the resonator due to the changes in the bearing temperature vary the natural frequency of the LC tank, so, the frequency of the circuit is a function of the measured temperature. As can be seen in Figure 31, the Meissner oscillator is a positive feedback oscillator that works by injecting energy into the resonator through the coil  $L_1$  and extracting the feedback by means of the coil  $L_2$ . Little energy is taken from the resonator to provide the voltage at the amplifier's input. To remain in oscillation, an adequate level of gain in the amplifier must to be provided. Resistors  $R_f$  and  $R_g$  determine the gain of amplifier.

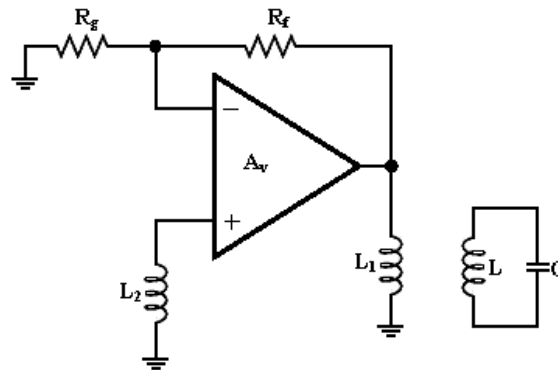


Figure 31. Schematic diagram for wireless temperature sensor based on a Meissner Oscillator.

This type of oscillator have several virtues such as: simplicity, low cost, absence of biasing resistors that reduce the quality factor  $Q$  of the resonator, reduced number of active devices generating noise, and lack of supply voltage ripple creating phase noise. However, a key disadvantage of this approach is that it was experimentally observed (see section 4.1.2) that the oscillation frequency depends not only on the device's temperature, but also on the separation between coils  $L$  and  $L_2$ . Proper operation of this device thus requires the distance between coils to remain nearly constant. It is difficult, if not impossible, to achieve this for applications where the two coils are moving with respect to each other.

### 3.3.2 Circuit design

As the sine wave amplitude of the resonator is controlled by the amplifier gain, this is the most important parameter in the design of the Meissner oscillator circuit. The inductive coupling between the coils must be large enough to allow the transmission to/from the sensing LC tank circuit. The voltage amount captured by the coil  $L_2$  is very low and hence it needs to be amplified by an adequate factor. So, the gain of the amplifier must be large enough to sustain the oscillations in the circuit. As it has been said before, the resistors  $R_g$  and  $R_f$  set the gain of the amplifier  $A_V$ . The threshold gain value was measured to be more than 10.

A temperature sensitive capacitive with an Y5V dielectric type was used for implementing the circuit. A single turn loop coil and the sensitive capacitor form the resonator sensing circuit as shown in Figure 32 (a). A 10 MHz natural frequency of operation was established for the present design.

Another consideration to have in account into the circuit design is the selection of an amplifier capable of operating at 10 MHz range. The MAX477 amplifier from MAXIM was selected because of its large bandwidth. Figure 32 (b) shows the amplifier and reception unit built for the present study.

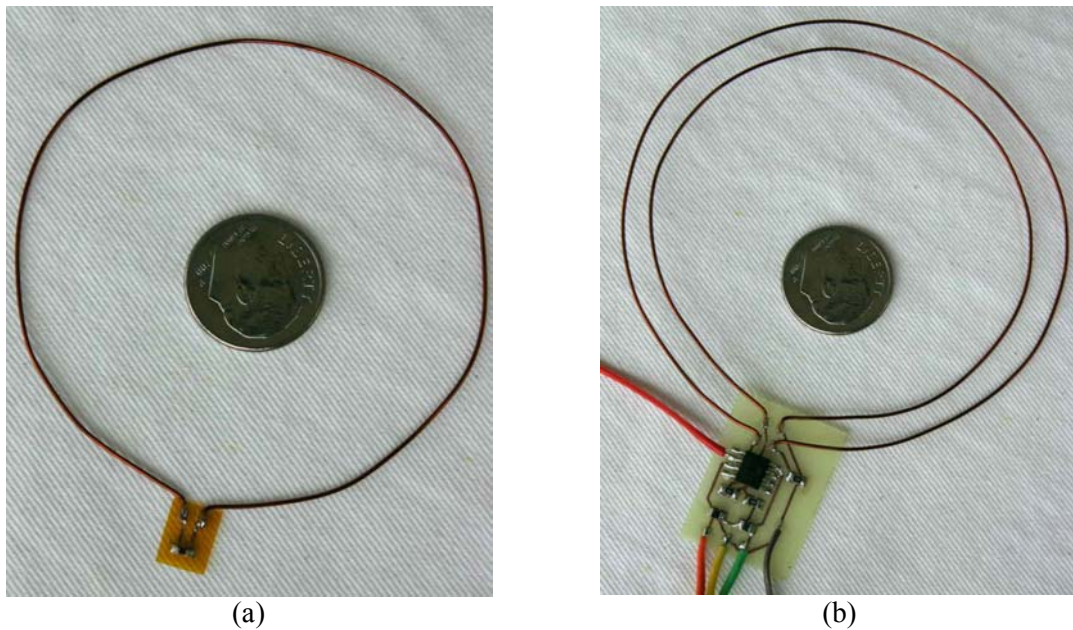


Figure 32. Wireless temperature sensor based on Meissner oscillator. (a) LC sensor unit and (b) amplifier and reception unit.

### **3.4 RADIO FREQUENCY IDENTIFICATION – BASED TEMPERATURE SENSOR**

#### **3.4.1 Principle of operation**

This approach is based on the principle of Radio Frequency Identification RFID, used in devices that are widely available on the market. Its main advantage is that the mechanism used to transmit the power is also used to receive the information from the sensor. Hence, only two antennas are needed. RFID devices have given popularity to passive (RF powered) telemetry systems for non-sensing applications [34-36]. Extending this technology to sensors would allow a whole range of new applications.

The main components of an RFID system are the reader and tag. The reader transmits a continuous RF carrier signal. When a tag enters the RF field of the reader, the tag receives energy to operate. Once the tag is energized by the transmitter, it modulates the carrier signal according to the data to be sent [22 - 23], [34]. Finally, the reader detects the modulated signal. For our case, the reader is also the RF power transmitter and the tag is the sensing circuit.

The most important issues in a RFID system design are their capability to give enough power to the wireless monitoring system and to recover the modulated signal. The theory that governs the RF powering technique was discussed in Chapter 2. The modulation technique known as backscatter modulation [34] can be described as a parallel LCR tank which represents the wireless monitoring system coupled magnetically with the remote powering and data receiving antenna as shown in the equivalent circuit model of Figure 33.

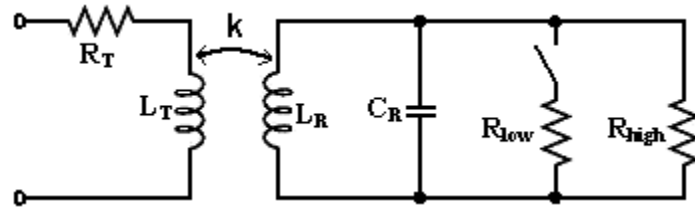


Figure 33. Circuit model for backscattering modulation technique

In Figure 33,  $R_T$  and  $L_T$  correspond to the resistance and inductance of the transmitting antenna, and  $k$  is the coupling coefficient between the coils. The modulated backscattering technique is implemented by switching between equivalent high- and low-load impedances (Figure 33). The load for the coupled wireless system is defined by  $R_{high}$  and  $R_{low}$  when the loading switch is open and closed respectively. In the power transmitting cycle, the transmitting powering coil sends an electromagnetic signal. This signal is then received by the antenna of the sensing circuit, which is tuned to the same frequency of the power transmitter by means of resonant  $L_R C_R$  circuit. In the information transmitting cycle, the modulated loading of the parallel LCR tank reflects an amplitude modulation (AM) on the carrier as showing in Figure 34. This modulated signal can be captured by an envelope detector in the power transmitter unit.

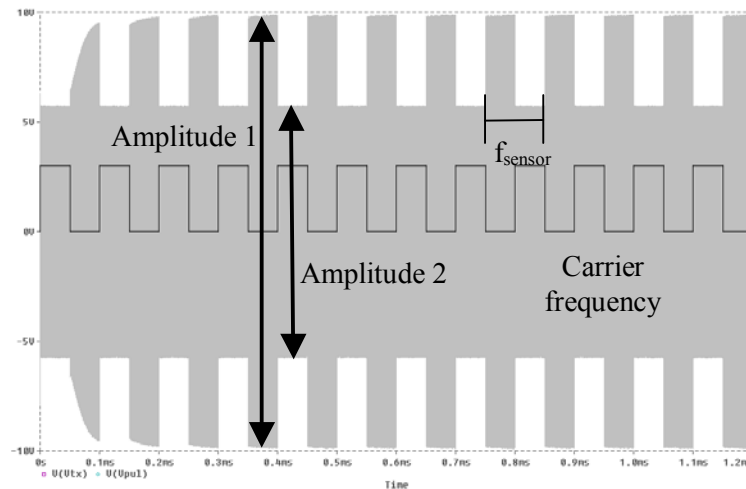


Figure 34. Waveform signal for the backscattering modulation (AM signal)

### 3.4.2 Circuit design

A schematic diagram for the RF powered wireless monitoring system designed in this approach is shown in Figure 35. The temperature sensor used in this system is an IC-temperature sensor LM60 from National Semiconductors [55] described in Section 3.2.1. The voltage signal from the transducer is digitized by the use of a voltage-to-frequency (V/F) converter, which was implemented with AD654 integrated circuit from Analog Devices [61]. The digitization of the transducer output is needed for enabling the backscattering modulation of the temperature data with the objective of sending this information to the power-transmitting/reception unit. The output frequency value of the V/F converter is governed by equation (26).

$$F_{\text{out}} = \frac{V_{\text{in}}}{(10\text{V})(R_f)(C_f)} \quad (26)$$

where  $R_f$  and  $C_f$  are used to set the frequency range in the output of the V/F converter. For our case these values were chosen to obtain a 5 kHz to 10 kHz frequency range using the input voltages ( $V_{\text{in}}$ ) given by the IC-temperature sensor according to Table 4.

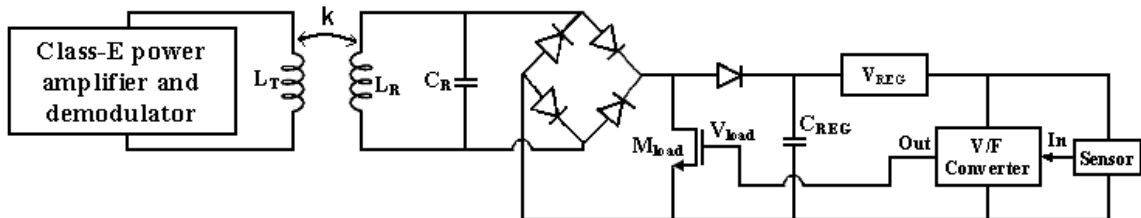


Figure 35. Schematic diagram for the RF powered wireless system based on RFID principle

The input admissible voltage values by the V/F converter are between 0 V and 1.6 V range. The digital frequency temperature data from the sensor can then be sent to the  $L_R C_R$  tank of the receiver unit for transmission by using modulation.

A class-E power amplifier, described in a detail form in Section 2.3.2 was used to generate the RF carrier signal and to energize the sensing circuit. The wireless system

includes a power receiver discussed in Section 2.2 which contains the LC resonator followed by a bridge rectifier as shown in Figure 35. Furthermore, with the objective of protecting the regulated signal from any power fluctuations caused by the load modulation a diode was added. Finally a voltage regulator is in charge to deliver energy to the sensor and to the V/F converter.

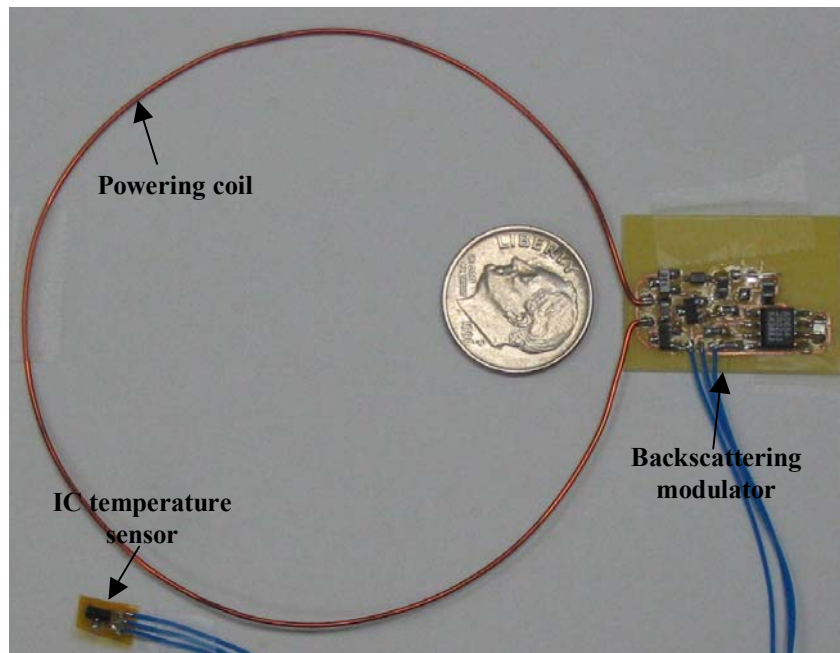


Figure 36. RF-powered wireless temperature sensor based on RFID principle.

The modulation is done using the digital output signal of the V/F converter loading in an active form the  $L_R C_R$  tank of the wireless system by means of controlling the switching of the transistor  $M_{load}$  in Figure 35. It is clear that the frequency of the output signal of the V/F converter is lower than the carrier frequency of the system. Figure 36 shows the RF powered wireless temperature monitoring system based on RFID principle developed in the present project.

## 3.5 FABRICATION OF THE SENSORS

### 3.5.1 Manufacturing process

The wireless systems developed in this thesis were built on Printed Circuit Boards (PCBs). As can be observed in the circuit implementations showed in Figures 23, 30, 32 and 36, the components responsible for non-temperature sensing tasks were placed in their own boards. In this way the sensing elements can to be attached to the measurement point without increasing the temperature of the active and passive components of the circuit. Only when the sensor was installed on a ball bearing all of the electronic components of the circuit were placed on the same board (see Figure 38).

Two types of copper clad were used in the fabrication process. The main circuit was manufactured using a FR4 laminate of 395  $\mu\text{m}$  with 305  $\text{g}/\text{m}^2$  (1  $\text{Oz}/\text{ft}^2$ ) of cooper. The transducers were placed over a copper clad laminate known as *Pyralux*<sup>®</sup>, which is a composite of *DuPont Kapton*<sup>®</sup> polyamide film with copper foil. Due to the simplicity of the sensor circuits a single layer circuit board is required. The *Pyralux*<sup>®</sup> used for this study, is the LF9110, it has 305  $\text{g}/\text{m}^2$  (1  $\text{Oz}/\text{ft}^2$ ) of cooper, over a *Kapton*<sup>®</sup> polyamide film of 25  $\mu\text{m}$  (1 mil) bonded with an adhesive layer of 25  $\mu\text{m}$  (1 mil).

The circuit pattern as shown in Figure 37 (a) was generated using the specialized CAD software Eagle<sup>®</sup>. A toner-transfer method was used to fabricate the printed circuit boards (PCBs), due to its low cost and implementation ease. The construction process is as follows: the image of the circuit was printed on the glossy side of a photo paper using a laser printer with high resolution. Once the board was completely clean and free from fingerprints, the photo paper was placed over the copper clad board with the glossy face down. Using a heat source and applying a small pressure on the paper and copper clad, the track pattern was transferred from the paper to the copper clad. Then the board was immersed in water. After 10 minutes, the paper dissolved and was removed from the copper board, leaving a toner-printed pattern on the surface of the board. The circuit

board was immersed in a Ferric Chloride etching solution, commercially available for etching of electronic circuit boards. Copper not protected by the toner reacted with the solution and was etched away. The desired copper pattern remained on the board. The board was washed with water and dried. The remaining toner was removed with acetone. The printed circuit board was finished by soldering the electronic components. Surface mount device (SMD) components were used. The SMD components were soldered onto the circuit board using conventional soldering methods. Figure 37 (b) illustrates a resulting PCB.

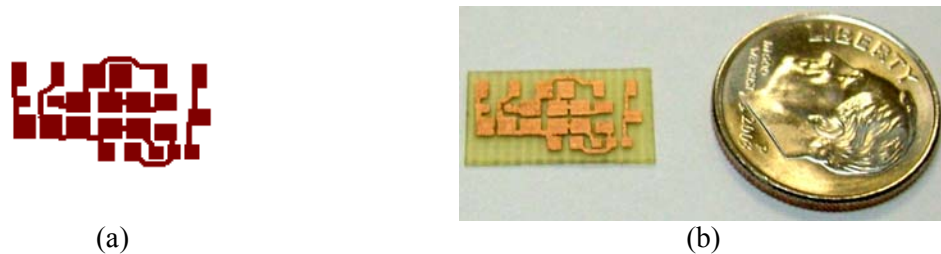


Figure 37. Pattern of a wireless temperature sensor circuit. (a) Eagle Pattern and (b) pattern implementation

### 3.5.2 Installation of wireless sensors on bearings

Once the printed circuit board was constructed using the method described in section 3.5.1, this was populated with the electronic components corresponding to each wireless system implemented. Figure 38 illustrates an RF-powered wireless temperature monitoring circuit populated with SMT electronic components. The developed wireless systems were installed on the bearings using a gluing component. Figure 39 shows a photo of the first version of the RF-powered wireless temperature monitoring circuit based on a Colpitts oscillator mounted on the cage of a tapered roller bearing.



Figure 38. Printed Circuit Board with SMT electronic components

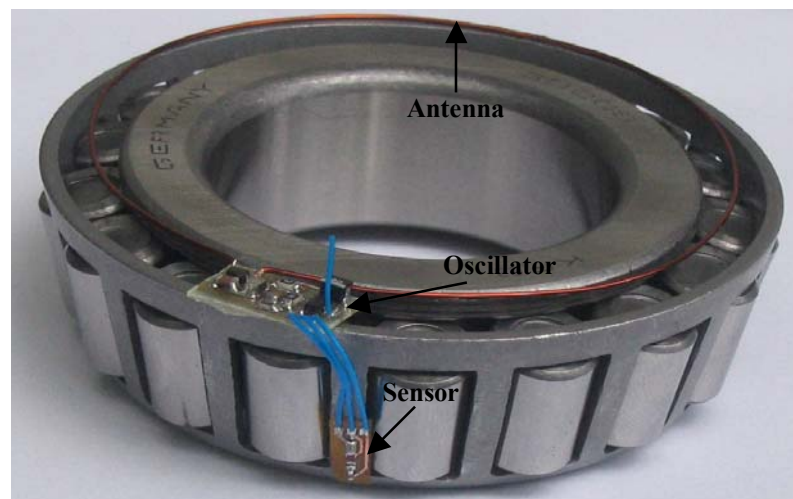


Figure 39. First version of the RF-powered wireless temperature sensor based on LC Colpitts oscillator installed on a tapered roller bearing

All the wireless temperature monitoring systems developed in the present thesis use a loop antenna to receive a power signal from the power transmitter unit. The loop wire antenna worked well while separated from a metal surface, but when it was placed on the bearing cage, the received power decreased greatly. To avoid this problem, an isolator material was placed between the cage and the loop wire antenna. Finally, a new version in which the loop wire antenna was changed by a PCB trace antenna was implemented.

This new implementation uses a copper substrate of 1.6 mm. This copper thickness separates the bearing surface and the antenna by enough distance to obtain adequate power levels in the sensing circuits. The inductance value of the new antenna was calculated to be the same than that in the loop wire antenna. Figure 40 illustrates the latest version of the RF-powered wireless temperature system which includes the new assembly.



Figure 40. Latest version of the RF-powered wireless temperature sensor based on LC Colpitts oscillator installed on a tapered roller bearing

An RF-powered wireless temperature monitoring system was implemented on a plastic-flexible PCB substrate described in section 3.5.1. This system was installed on a ball bearing as shown in Figure 41. For this case, the loop wire antenna was changed to a PCB trace antenna. Furthermore, the transmitted power had to be greatly increased because of the great losses that occur within the bearing.



Figure 41. RF-powered wireless temperature sensor based on LC Colpitts oscillator installed on a ball bearing built over a polyimide film

### 3.6 SUMMARY

This chapter has presented the development of several circuits for an RF-powered and wireless temperature data transmission system. All of the circuits were implemented using SMT devices and a simple manufacturing process. The RF powering technique discussed in Chapter 2 was used to deliver the energy needed by the circuits to properly operate. Once the circuits were installed on bearings, great power losses were observed because of proximity of the metal parts. To avoid this problem the transmitted power was increased and an insulating material was placed between the power receiving antenna and the surface of the bearing. The circuits have been fabricated and tested. Results will be given in Chapter 4.

## **4. IMPLEMENTATION RESULTS**

This chapter presents the temperature calibration results obtained from various RF-powered wireless monitoring systems described in Chapter 3. The experimental setup used for the calibration and the testing procedure are described. Results obtained for the wireless sensors developed in the present thesis are compared. Finally, results from a realistic test in which the RF-powered temperature wireless system based on a Colpitts oscillator described in chapter 3 was used on an operational (rotating) ball bearing are discussed.

### **4.1 SENSOR CALIBRATION**

#### **4.1.1 Calibration procedure and setup**

The devices described in Chapter 3 were calibrated with the objective of experimentally determining the relation between the temperature of a test setup and the sensor response. The setup used to collect temperature wireless data consisted of a receiving antenna, an Agilent 54622 oscilloscope and a data acquisition board as shown in Figure 42. The data receiving antenna was located in the vicinity of the sensor.

For the Colpitts-, VCO- and Meissner-based sensors, a GPIB data acquisition card was used to transfer the sensor information in the time domain to a PC. With a LabView program (see Figure 44) a band-pass filter was applied to the acquired information with the objective of eliminating the data that do not contain temperature information. The cutoff frequencies of the filter were determined according to the operating frequency range of each wireless system. Then a spectral analysis was performed on the filtered data and the power spectrum peak's frequency was extracted. Finally, this frequency value was related with a temperature value after calibration.

It is important to point-out that the data-receiving antenna depends on the operational principle of each sensor. For the sensor based on a Colpitts oscillator, the receiving antenna was an AM radio antenna with ferrite core. The sensor based on a VCO used a simple wire loop of 80 mm of diameter as receiving antenna. For the Colpitts- and VCO-based sensors, the oscilloscope was attached to the respective receiving antenna and used to determine the frequency spectra of the sensor signal, as shown in Figure 43. The FFT algorithm was used to calculate the spectra, which clearly showed two peaks: one at 10 MHz corresponding to the signal used to power the circuit, and another one that corresponds to the temperature dependant oscillator signal. It was then possible to monitor the oscillator frequency carrying the temperature information. For the Meissner oscillator circuit, the output of the amplifier is connected to the oscilloscope for the subsequent analysis. For the sensor based on RFID principles, the transmitter power antenna is used as a data receiving coil as well, hence, the oscilloscope is connected to the output of the class-E power amplifier.

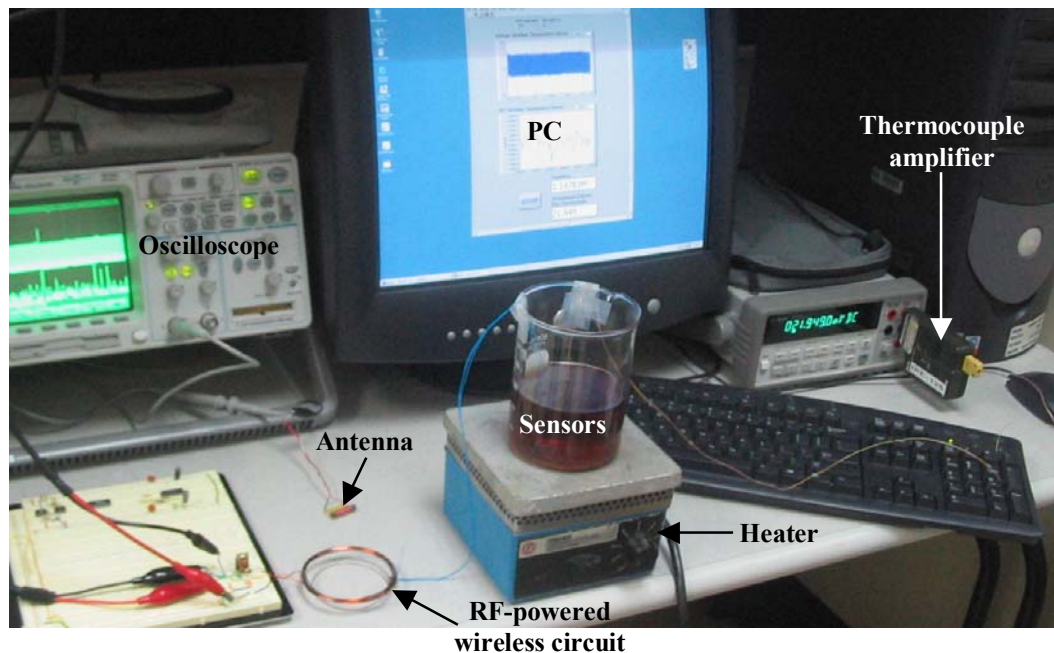


Figure 42. Sensor calibration setup

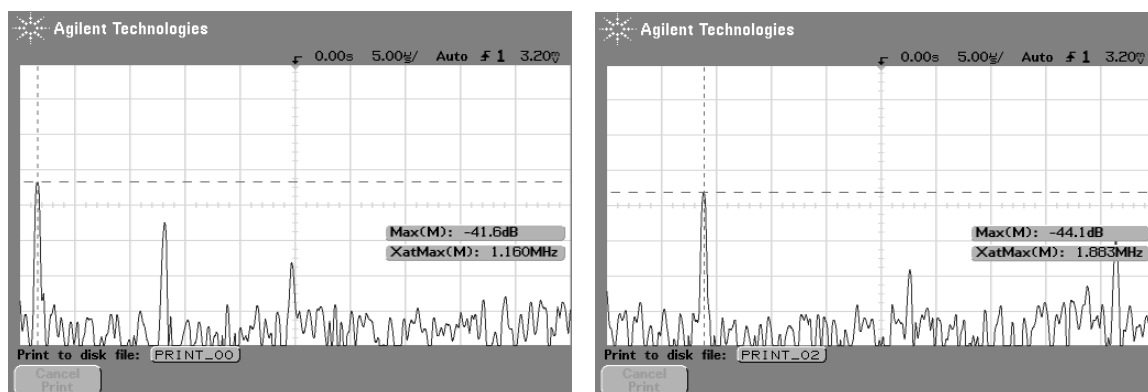


Figure 43. FFT of received signals for temperatures of 25°C (1.160 MHz) and 70°C (1.88 MHz), respectively when using the wireless sensor based on a Colpitts oscillator.

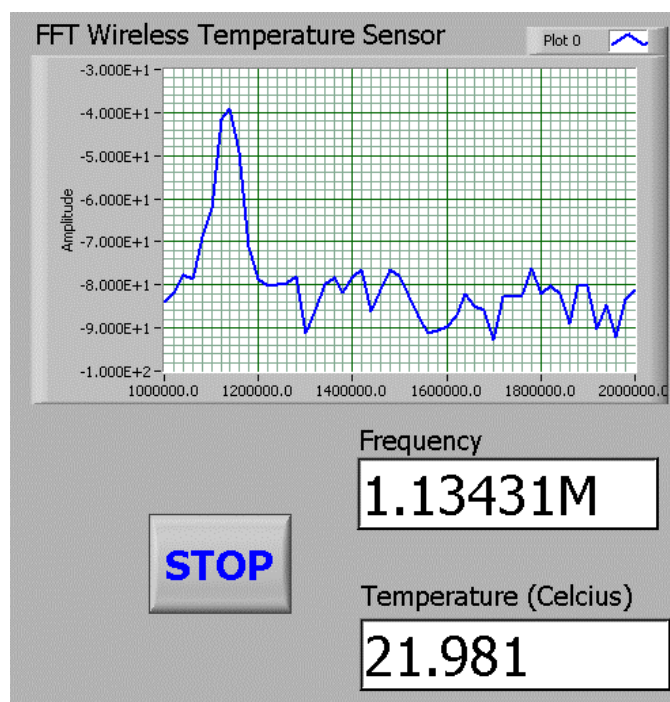


Figure 44. Display of the Labview program used for temperature data acquisition and analysis

To calibrate the wireless sensors, the sensing elements of each RF-powered wireless temperature sensor were immersed in a 300 ml beaker filled with engine oil that was placed over a hot plate as it can be seen in Figure 42. The oil temperature was independently measured with a K-type thermocouple. Sensor signal and thermocouple reading were simultaneously captured by a Labview program, as shown in Figure 44.

Hence, the program described above was conditioned to receive two channels: one for the wireless sensor and another for the thermocouple. The reservoir was placed over the hotplate and the temperature was gently increase and decrease from 20 °C to 80 °C. Each time the temperature set point was modified, the system was allowed to reach steady state before recording the calibration point. Once the data from both sensors were recorded, calibration curves were generated, as is shown in the next section.

#### **4.1.2 Calibration results**

Figure 45 shows the measured frequency versus temperature for an RF-powered wireless temperature sensor based on a Colpitts oscillator. A least-square linear fitting of the data yields a resolution of 15.7 kHz per degree Celsius, with an offset of 784 kHz. Since the largest departure from linearity is about 25 kHz, a linear approximation would yield an accuracy of about 2 degree Celsius. Better accuracy can, of course, be achieved a higher degree approximation is used. Alternatively, a look-up table can also be employed.

A test was performed to study the stability of our circuit. The temperature was increased and reduced over a period of time, while monitoring the thermocouple and wireless sensor readings. The two sets of data are compared in Figure 46. It can be observed that the two sets are in very good agreement, demonstrating that the wireless sensor displays good stability.

Figure 47 and Figure 48 show the calibration curves for the RF-powered wireless temperature sensor based on a VCO. Again, the thermocouple and wireless sensor data were recorded while the temperature of the calibration oil was increased and decreased on a time interval. An analysis of these data yields a sensitivity of 35.5 kHz per degree Celsius. Furthermore, from Figure 48, the stability of the sensor can be demonstrated.

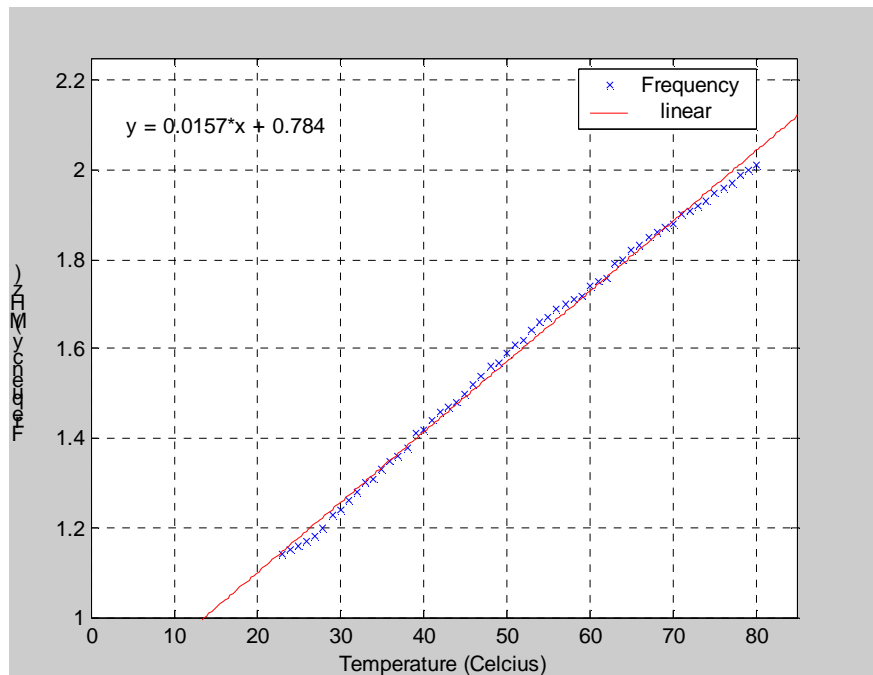


Figure 45. Calibration curve for a wireless temperature sensor based on a Colpitts oscillator

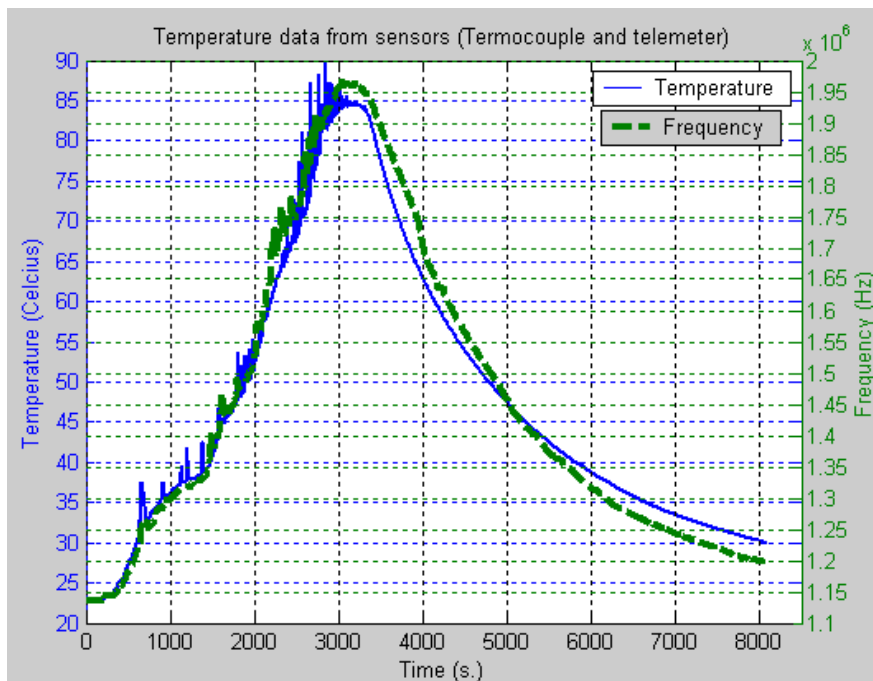


Figure 46. Temperature and frequency history respectively for calibration of the wireless temperature sensor based on a Colpitts oscillator

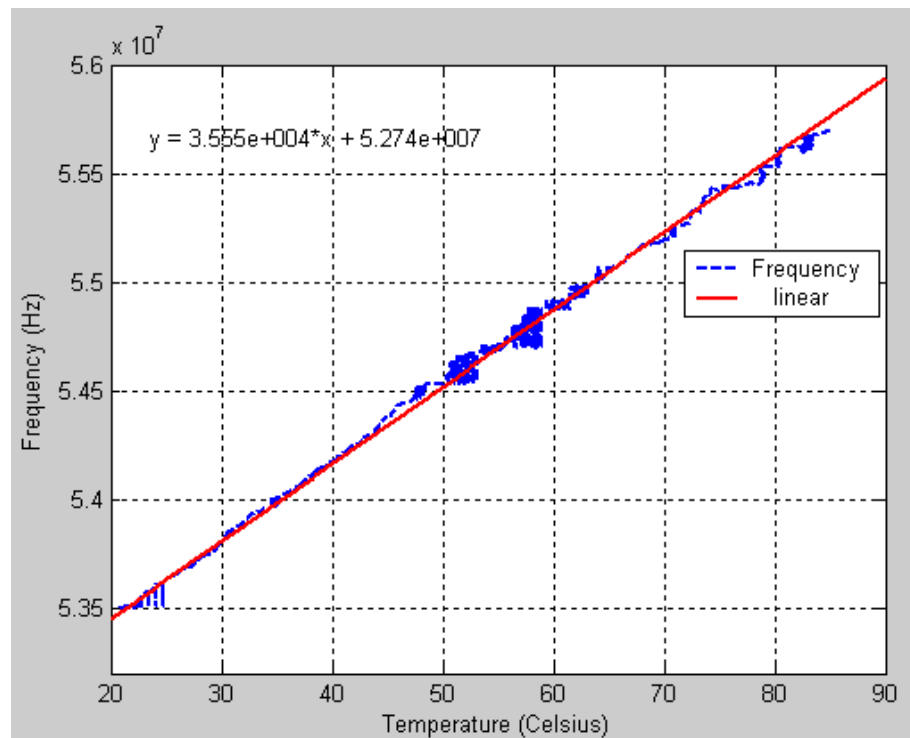


Figure 47. Calibration curve for a wireless temperature sensor based on a VCO

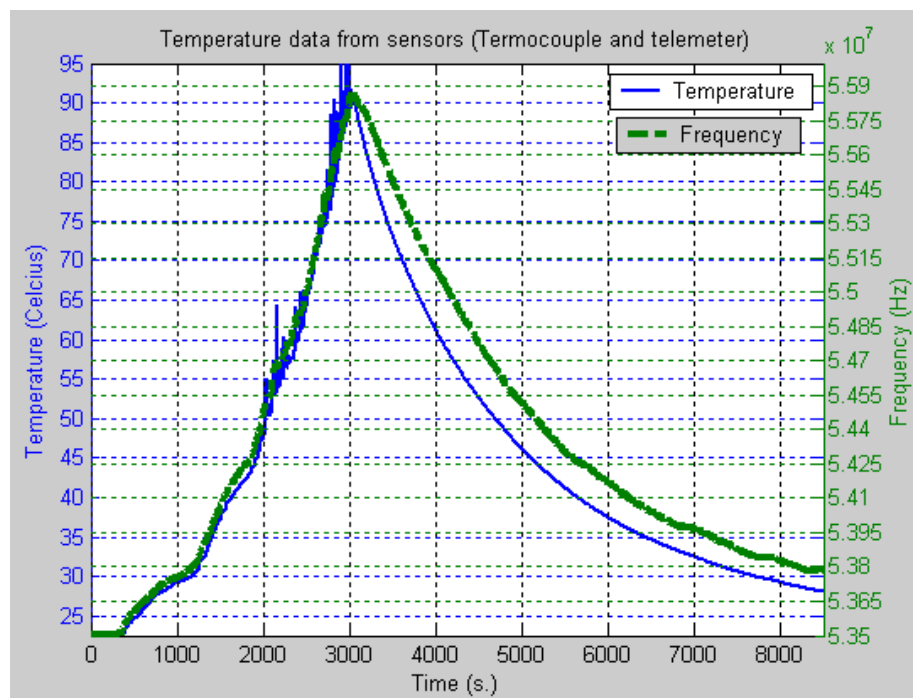


Figure 48. Temperature and frequency history respectively for calibration of the wireless temperature sensor based on a VCO

The calibration results for the wireless sensor based on a Meissner oscillator are showed in Figure 49 and Figure 50. After making an analysis of these data, an approximated resolution of 180 kHz per degree Celsius was found. The frequency of this sensor is highly dependent of the distance between the coils, so even small disturbances in the distance parameter affects the behavior of the sensor. The calibration results presented were taken with a fixed distance of 1 cm between the coils.

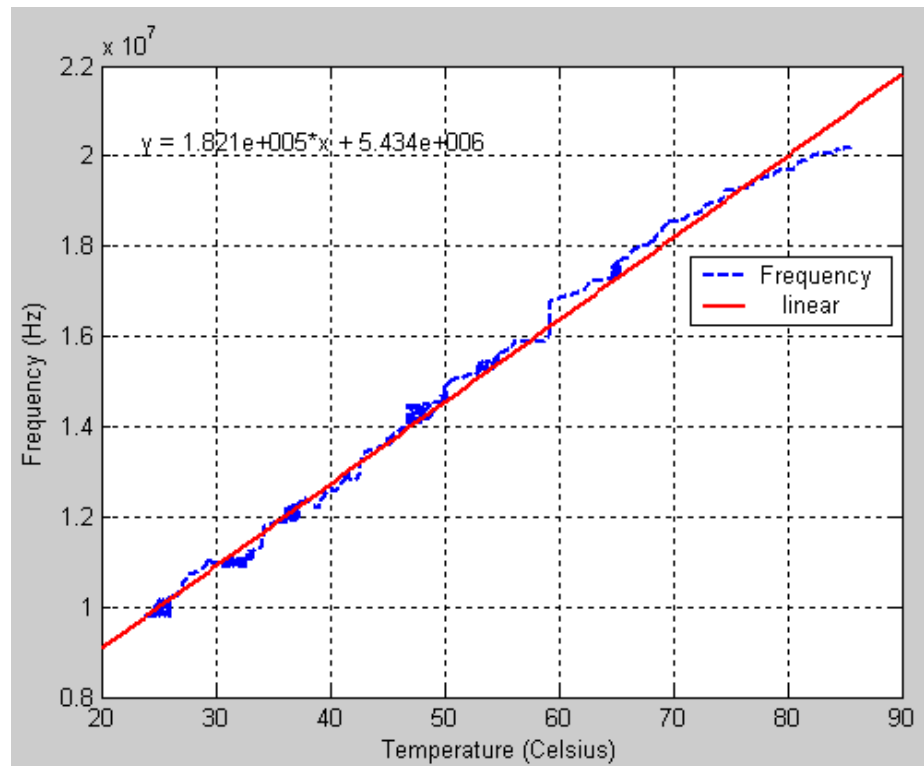


Figure 49. Calibration curve for a wireless temperature sensor based on a Meissner Oscillator

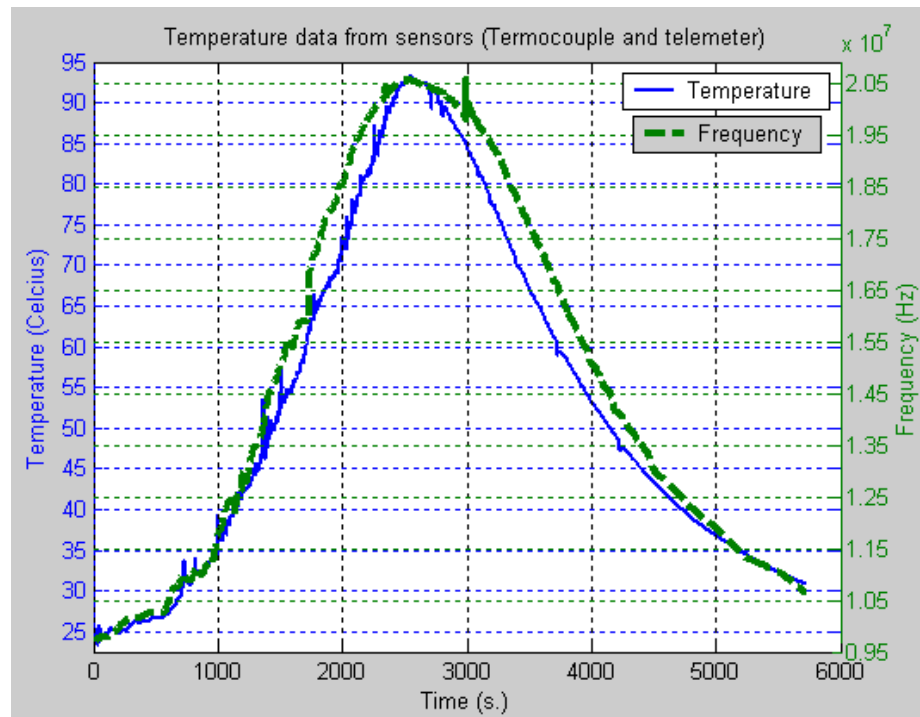


Figure 50. Temperature and frequency history respectively for calibration of the wireless temperature sensor based on a Meissner oscillator

For the RF-powered wireless sensor based on the RFID principle only three point-temperature measurements were taken because of the outputs of the transducer and the V/F converter are both linear as it was said in section 3.4. Figure 51 shows the acquired signals for 23°C, 35° and 90°C temperature points. The calibration curve for this sensor is showed in Figure 52. After executing a least-square linear fitting of the data, the resolution found was 61.44 Hz per Celsius degree with an offset of 4285 Hz. The temperature readings were chosen to be in the limits of the temperature range and a middle point between them with the objective of verifying the linearity of the device.

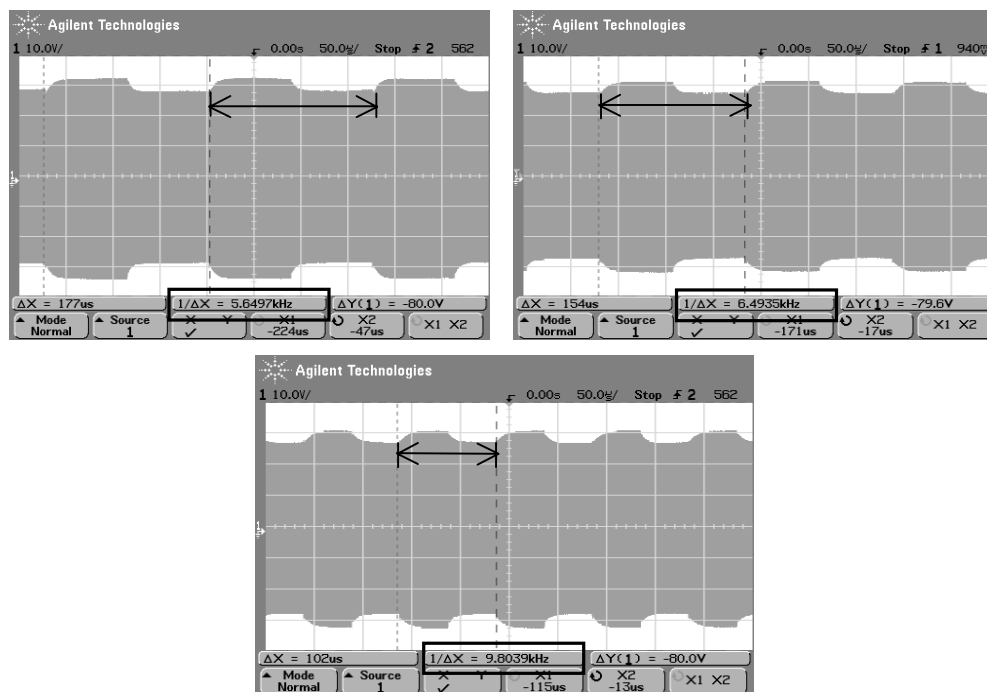


Figure 51. Acquired calibration signals for the RF-powered wireless temperature sensor based on RFID principle. (Signals recorded for 23°C, 35° and 90°C respectively)

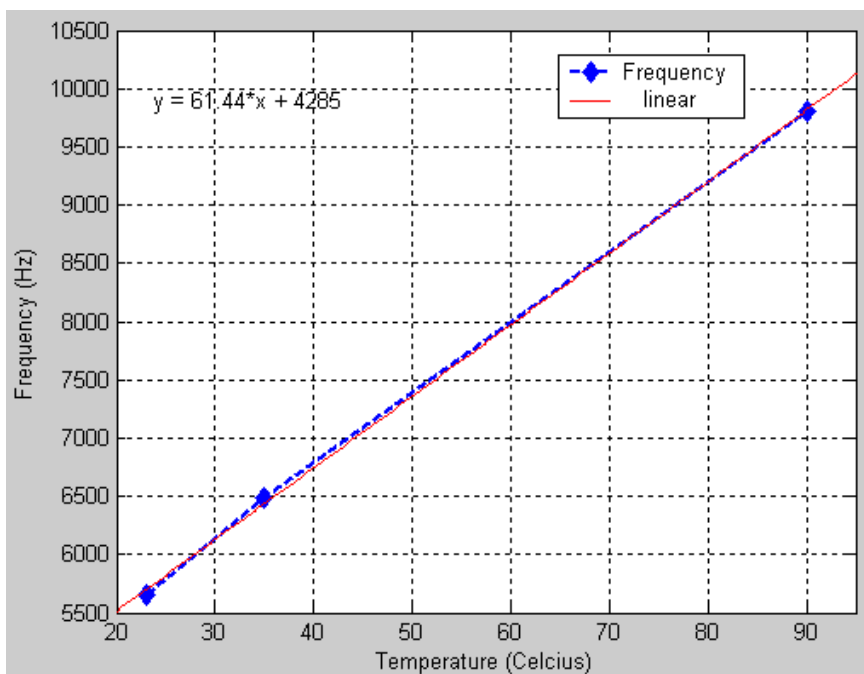


Figure 52. Calibration curve for the RF-powered wireless temperature sensor based on RFID principle

From the calibration curves we can conclude that the developed sensors have an approximately linear behavior for the bearing operation temperature range (20°C to 80°C). Table 5 summarizes the main characteristics obtained from calibration. The stability of the Colpitts oscillator-based sensor, VCO-based sensor and RFID sensor was verified. The frequency behavior if the Meissner oscillator-based sensor presents a high dependence on the distance between the coils, however as shown in Table 5 this sensor has the highest resolution. All of the developed sensors could be used to temperature monitoring within bearings if the miniaturization is achieved. Although the RFID based wireless sensor has the lowest resolution, it uses only a pair of antennas to make the main tasks of the system. Furthermore this principle is compatible with modern wireless technologies. However the number of components of this solution is large.

Table 5. Comparison between the wireless sensors

Sensor principle	Transducer type	Temperature range	Frequency range	Resolution
Colpitts Oscillator	Capacitive	20°C to 85°C	1.16 MHz to 2 MHz	15.7 kHz /°C
VCO	IC-temperature sensor	0°C to 125°C	53 MHz to 56 MHz	35.5 kHz /°C
Meissner Oscillator	Capacitive	20°C to 80°C	9 MHz to 21 MHz	180 kHz /°C
RFID	IC-temperature sensor	0°C to 125°C	5.6 kHz to 15 kHz	61.4 Hz /°C

Table 6. Capture range of temperature data for each wireless sensor principle

Sensor principle	Data receiving antenna	Capture range of data
Colpitts Oscillator	Ferrite core AM radio coil	Up to 5 cm.
VCO	Loop wire	Up to 8 cm
Meissner Oscillator	Loop wire	Up to 1 cm
RFID	Loop wire (used also to transmit power)	same as the powering range (3 cm to 5 cm)

Within the calibration tests, the capture range of the temperature data was observed as well. The range obtained for each sensor was summarized in Table 6. It is important to

point-out that this range was obtained under controlled, static calibration conditions, and as such it should be larger than the usable distance range obtained with the sensors installed on a bearing.

## **4.2 TEMPERATURE MONITORING ON AN OPERATING BEARING**

A lathe machine was used to carry out an experiment on a ball bearing. The setup is shown in Figure 53. The objective of the experiment was to verify the operability of a wireless device on a ball bearing for realistic operational conditions. In the experiment the Colpitts Oscillator-based sensor was used to monitor the temperature of ball-cage in a ball bearing as a function of speed. Figure 41 shows the test ball bearing instrumented with the RF-powered wireless temperature sensor described in section 3.1. The instrumented bearing was mounted on a spindle of the lathe; the spindle was used to rotate the bearing. An axial shaft was used to add load to the bearing. The spindle speed can be varied by discrete quantities, so the temperature for several speeds was registered after 10 minutes of machine operation for each velocity value. Two tests were done: one without load and another with a 20 pound load placed on the half of the shaft.

Figure 54 shows the temperature behavior within a ball bearing as a function of the speed under the two different load conditions. It can be observed that higher operating speeds cause the bearing to operate at higher temperatures. Adding load increases the temperature as well.

An overload condition can be detected using this RF-powered wireless system. These tests allowed us to evaluate the use of this technology for the temperature monitoring in bearing applications. The feasibility of monitoring the bearing-cage temperature, while the bearing is operating, using the wireless sensor based on the Colpitts oscillator was demonstrated by these results.

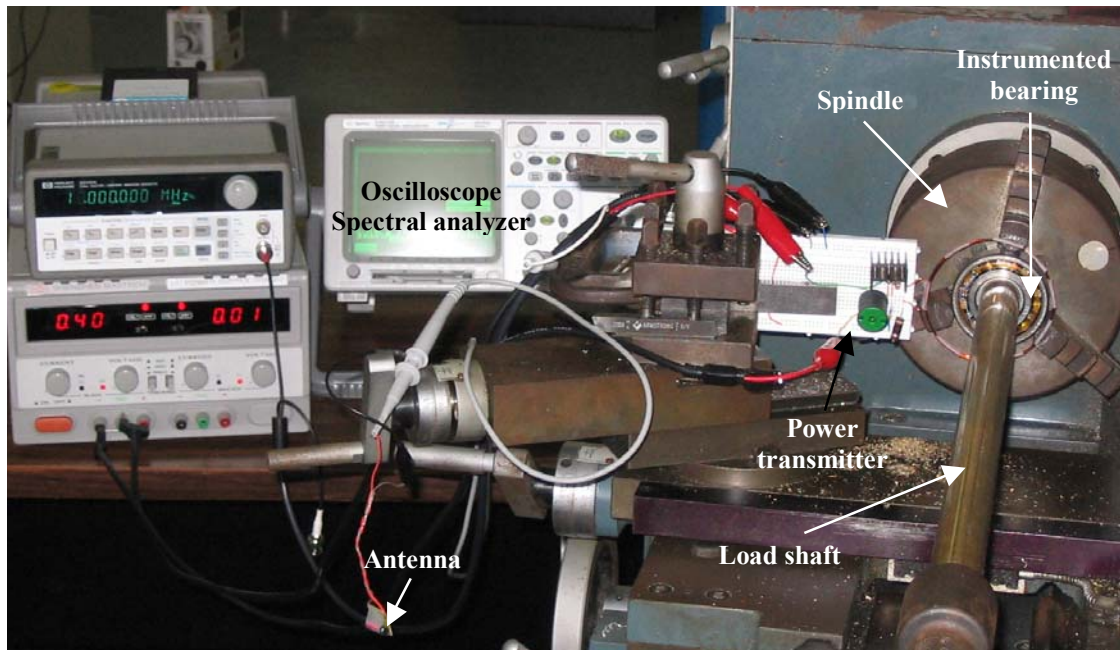


Figure 53. Experimental setup for real test of a ball bearing instrumented with an RF-powered wireless temperature sensor

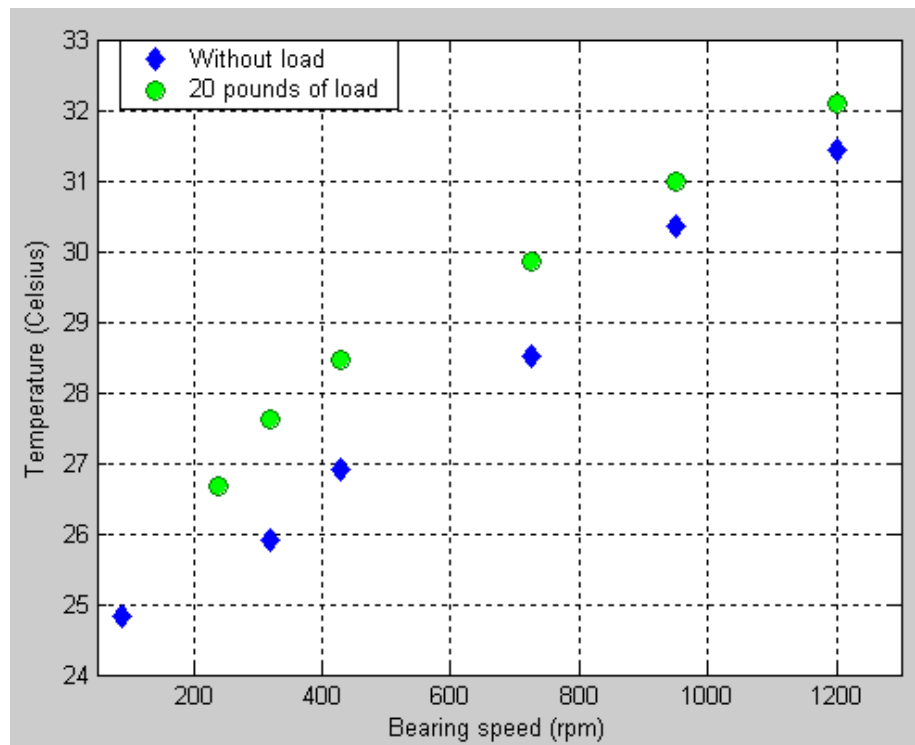


Figure 54. Bearing temperatures under several rotation speeds and two load conditions

Other tests were carried out in which the historical behavior of the cage temperature was recorded for different operational conditions of a ball bearing. The setup showed in Figure 53 was used here to measure the bearing cage temperature. GPIB card was used to acquire the data using a laptop computer. Two different operational speeds (1200 rpm and 1550 rpm) and two load conditions (25 and 45 pounds) were used for these tests. Figure 55 and Figure 56 show the temperature behavior for each case. For these measurements the lubricant was almost completely retired from the bearing with the objective of increasing the temperature, which normally remains low for the loads used. Each test was conducted until a reasonably stable temperature was reached; then the machine was stopped. The cooling down process was recorded as well.

These results show that the RF-powered wireless temperature sensors developed in this thesis can be used to perform dynamic measurements on operational bearings. The time and temperature resolutions obtained in the above tests are adequate to detect abnormal conditions in real-time. Thus we can conclude that these wireless sensors may provide an effective method to identify the possibility of a catastrophic bearing failure, thus enabling its prevention.

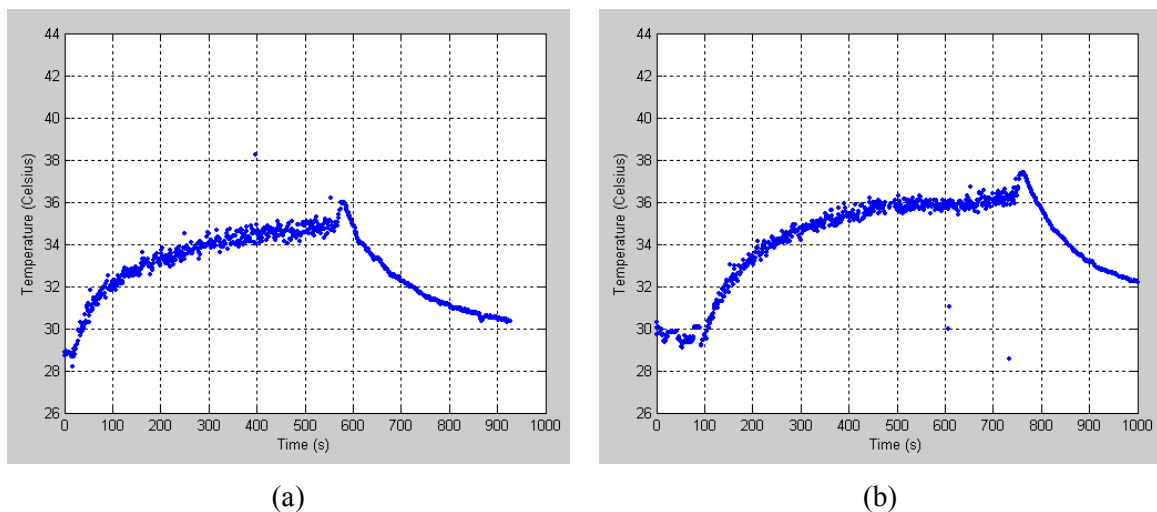


Figure 55. Cage temperature behavior of the bearing operating at 1200 rpm with a load of (a) 25 pounds and (b) 45 pounds

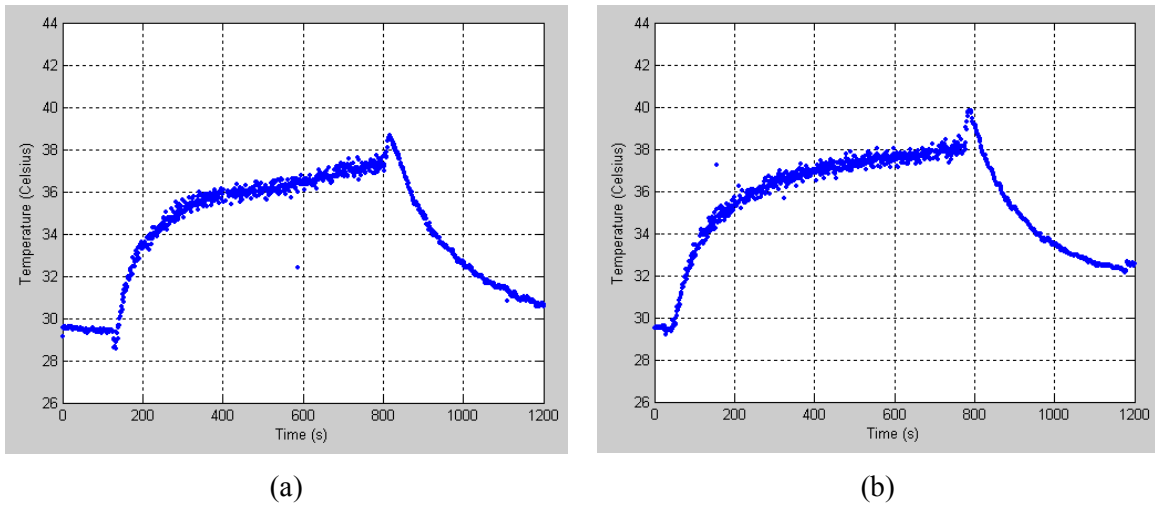


Figure 56. Cage temperature behavior of the bearing operating at 1550 rpm with a load of (a) 25 pounds and (b) 45 pounds

## 5. CONCLUSIONS

The contribution of the present work is the development of effective means to measure temperature within bearings (ball and roller types) in places closer to the heat sources (balls and bearing cage). While in previous published research the bearing temperature was measured at fixed races, the sensors developed in this thesis allow the monitoring of the cage temperature. Because the cage is moving relative to the fixed races, direct wiring of the sensing circuit is not possible. The sensors described in this document operate without a wired connection; they are remotely-powered and transmit data wirelessly. Since the ball bearing cage temperature has been identified as a variable closely related to bearing health, the sensors developed in this thesis provide an effective way of monitoring the bearing health while the device is in operation.

All the sensors developed in this thesis were powered via an RF signal. An inductively RF energy transmission system, consisting of two magnetically coupled coaxial loop wire inductors, has been implemented and used to power the wireless sensors. A high-efficiency class-E power amplifier was designed and used to send enough power to operate the sensor circuits. The power transmitter was driven at a frequency of 10 MHz. The implemented systems are based on two signals: one to send power and another used to transmit the temperature data to a receiving antenna for further analysis.

An optimization of the inductive link design was performed using classical electromagnetic models. Several design considerations for the inductive link can be extracted in order to maximize the powering distance of the receiver circuit such as: maximize mutual inductance by maximizing coil geometry, maximize the primary coil current by increasing the transmitter voltage, use low power and low voltage operated circuit at receiver. The theoretical analysis provided a powerful tool that allowed reduced design time and provided insight about the operation of these devices.

In the RF-powered wireless sensor based on a tuned Colpitts oscillator developed in this thesis, a pair of miniaturized temperature sensitive capacitors was integrated into a simple inductor-capacitor (L-C) oscillator as sensing elements. The oscillator was used as a telemeter circuit that transmitted the temperature data to a ferrite coil receiving antenna for computer analysis. A second version of an RF-powered wireless sensor was developed using an integrated Voltage Controlled Oscillator. In this second circuit the output voltage of an IC-temperature sensor controls the output frequency of the VCO. The data receiving antenna was a simple wire loop. A linear responses and good resolutions of the instruments were obtained using these devices.

A third wireless sensor, based on the same ideas used in Radio Frequency Identification (RFID) technology, was designed and developed. This device used a class-E amplifier for power transmission. The same antenna that transmitted power was used to receive the temperature data, which was coded using Amplitude Modulation. Although this sensor displayed the lowest resolution, in our view it represents a promising alternative because it is based on a well-tested and reliable technique that has been used in many security and tracking applications.

Although the two-component sensor based on a Meissner oscillator principle has the highest resolution of the developed instruments, its frequency is very sensitive to the distance between coils, and small distance variations have a detrimental effect over the performance of the circuit. This is a disadvantage for the use of this wireless system in the bearing application because, since the bearing is in motion, it will be difficult to keep the distance between the two coils constant.

Losses in the received power were observed when the circuits were installed on bearings because of the vicinity metal parts. To operate the battery-less circuits, the transmitted power was increased and an isolating material was added between the powering receiving coil and the surface of the bearing.

The sensor circuits described here provide feasible solutions for the monitoring of bearing health. Dupont *Kapton*® thick film substrate and Surface Mount Devices (SMD) were used to fabricate the compact circuits needed to allow installation inside a bearing. The sensor calibration shows that all prototype sensors have a relatively linear response, and display stable operation with good sensitivity. A trade-off between stability, resolution and size is needed to choose the sensor once the restrictions of the application are known. A ball bearing instrumented with a miniaturized Colpitts oscillator-based wireless sensor built over a polyimide film was used to conduct a test under real bearing operation so that the functionality of the developed circuits was verified.

Although the devices developed in this thesis have been tested and their functionality for measuring temperature in bearings have been verified, they are experimental prototypes that need further improvements to transform them into a solution that can be deployed in the field. Our results for the VCO-based wireless sensor indicate that the operational distance range can be increased by using higher transmission frequencies. New devices operating at higher frequencies should be explored. The RF-powered wireless sensor based on a VCO should be miniaturized and tested to evaluate their behavior under real bearing operation.

The size constraints imposed by the bearing make it difficult to develop a final solution using discrete components. For the LC Colpitts oscillator-based and the RFID-based sensors, integration of the whole circuit within a chip might provide a more suitable solution, albeit at an increased cost. Since the two-component sensor based on a Meissner oscillator has a small size, it is important to make additional studies to look for ways of dealing with the frequency dependence on the distance between coils.

Finally, although the equipment used to process the received temperature data such as a spectrum analyzer and computer data acquisition system provided an effective experimental platform to develop the prototypes presented here, a handheld circuit can and should be develop.

## BIBLIOGRAPHY

- [1] T. A. Harris. “Rolling Bearing Analysis”. Second edition. New York : Wiley, 1984. 565 pp.
- [2] Valonen, Kai Investigation of Rail Accidents. International Comparison. 2000. <http://www.onnettomuustutkinta.fi/uploads/rdpaocglrpk.pdf>. Active November 2002.
- [3] Transport Canada. TP 12691-E, Hot Bearing Detector Study Railway Safety Directorate, 1996. [http://www.tc.gc.ca/railway/ENGLISH/HOT\\_BEARING/hbdrp6\\_1.htm](http://www.tc.gc.ca/railway/ENGLISH/HOT_BEARING/hbdrp6_1.htm). Active November 2002.
- [4] J. E. Cline, J. R. Bilodeau, R. L. Smith. “Acoustic wayside identification of freight car roller bearing defects”. Railroad Conference, 1998. Proceedings of the 1998 ASME/IEEE Joint , 1998. pp. 79 –83.
- [5] M.A. Fonseca, J.M. English, M. Von Arx, M.G. Allen, “Wireless micromachined ceramic pressure sensor for high-temperature applications”, Journal of Microelectromechanical Systems, Vol. 11, Issue 4, Aug. 2002, pp. 337 -343
- [6] R.X. Gao, Y. Jin, R.O. Warrington, “Microcomputer-based real-time bearing monitor”, IEEE Transactions on Instrumentation and Measurement, vol. 43 Issue: 2, April 1994. pp. 216 –219
- [7] E. Romero, “Wireless temperature sensor for bearing health monitoring”, Master thesis, Mechanical Engineering department, University of Puerto at Mayaguez, May 2003, 78p.
- [8] C. Wang, R.X. Gao, “A virtual instrumentation system for integrated bearing condition monitoring”, IEEE Transactions on Instrumentation and Measurement, vol. 49 Issue: 2, April 2000. pp. 325 –332
- [9] Industrial applications of topology and shape optimization with TOSCA and ABAQUS. 2001. ABAQUS User’s conference pp. 1-11. 2001 International CIRP Design Seminar/6.-8. Jun 2001, Stockholm, Sweden. [http://www.fe-design.com/publications/papers.01/2001-05-30\\_FED\\_alusuisse\\_INA\\_.pdf](http://www.fe-design.com/publications/papers.01/2001-05-30_FED_alusuisse_INA_.pdf) . Active November 2002.
- [10] The Timken Company. Website: <http://www.timken.com/products/bearings>. Active March 2004.
- [11] Omni Instruments. Website: <http://www.omniinstruments.co.uk/radiotel/radiotel.html>
- [12] MicroStrain® Microminiature Sensors. Website: <http://www.microstrain.com/>
- [13] D. Krantz, J. Belk, P.J. Biermann, J. Dubow, L.W. Gause, R. Harjani, S. Mantell, D. Polla, P.Troyk, “Project Update: Applied Research on Remotely-Queried Embedded

- Microsensors”, Proceedings of SPIE – The International Society for Optical Engineering, v.3673, 1999, pp. 157-164.
- [14] C. Hautamaki, S. Zurn, S.C. Mantell, D.L. Polla, “Embedded Microelectromechanical Systems (MEMS) for Measuring Strain in Composites”, In Journal of Reinforced Plastics and Composites, v.19, No.4, 2000, pp.268-277.
- [15] O. Akar, T. Akin and K. Najafi, “A wireless batch sealed absolute capacitive pressure sensor”, Sensors and Actuators A 95 (2001), pp. 29 – 38.
- [16] K.J. Cho, H.H. Asada, “Wireless, battery-less stethoscope for wearable health monitoring”, Proceedings of the IEEE 28th Annual Northeast Bioengineering Conference, 20-21 April 2002, pp. 187 -188
- [17] T.J Harpster, B. Stark, K. Najafi, “A passive wireless integrated humidity sensor”, The 14th IEEE International Conference on Micro Electro Mechanical Systems, 2001. MEMS 2001, 21-25 Jan 2001, pp. 553 -557.
- [18] M. Hakoziaki, H. Oasa, H. Shinoda, “Telemetric Robot Skin”, IEEE International conference on Robotics & Automation, Detroit, Michigan, May 1999, pp 957 – 961.
- [19] M. Hakoziaki and H. Oasa. “Wireless Tactile Sensing Element Using Stress-Sensitive Resonator”, IEEE/ASME Trans. on mechatronics, vol. 5, No. 3, pp 957 – 961, Sep. 2000.
- [20] T. Eggers, J. Draeger, K. Hille, C. Marschner, P. Stegmaier, J. Binder, R. Laur, “Wireless intra-ocular pressure monitoring system integrated into an artificial lens”, 1st Annual International Conference On Microtechnologies in Medicine and Biology, 2000 , 12-14 Oct. 2000, pp. 466 -469.
- [21] K. Van Schuylenbergh, R. Puers, “Self Tuning Inductive Powering For Implantable Telemetric Monitoring Systems”, Transducers '95, The 8th International Conference on Solid-State Sensors and Actuators 1995 and Eurosensors IX, Vol. 1, June 25-29, 1995, pp. 55 -58
- [22] S. Chatzandroulis, D. Tsoukalas, “Capacitance to frequency converter suitable for sensor applications using telemetry”, Proceedings of ICECS '99, The 6th IEEE International Conference on Electronics, Circuits and Systems, Vol. 3, 5-8 Sept. 1999, pp. 1791 -1794.
- [23] D. Dudenbostel, K.-L Krieger, C. Candler, R. Laur, “A new passive CMOS telemetry chip to receive power and transmit data for a wide range of sensor applications”, International Conference on Solid State Sensors and Actuators, 1997. TRANSDUCERS '97 Chicago, 1997, Vol. 2, 16-19 June 1997, pp. 995 -998
- [24] A. Bayrashev, A. Parker, W. P. Robbins and B. Ziaie. “Low frequency wireless powering of Microsystems using piezoelectric-magnetostrictive laminate composites”, The 12<sup>th</sup> International Conference on Solid State Sensors, Actuator and Microsystems, Boston, June 8-12, 2003, pp 1707 – 1710.

- [25] Y. Kuwana, N. Ando, R. Kanzaki and I. Shimoyama, "A Radiotelemetry System for Muscle potential Recordings from Freely Flying insects", Proceedings of The First Joint BMES/EMBS Conference Serving Humanity, Advancing Technology 1999, Atlanta, GA, USA, pp. 846
- [26] S. Takeuchi and I. Shimoyama, "An RF-Telemetry System with Shape Memory Alloy Microelectrodes for Neural Recording of Freely Moving Insects", First Annual International IEEE-EMBS Special Topic Conference on Microtechnologies in Medicine & Biology, 2000, October 12 – 14, 2000, pp. 491 – 496.
- [27] G. Vandevoorde and R. Puers, "Wireless energy transfer for stand-alone systems: a comparison between low and high power applicability", Sensors and Actuators A 92, 2001, pp. 305 – 311.
- [28] T. Akin, B. Ziaie, and K. Najafi, "RF Telemetry Powering and Control of Hermetically-Sealed Integrated Sensors and Actuators," Digest, IEEE Solid-State Sensors and Actuators Workshop, pp. 145-148, Hilton Head, SC, June 1990.
- [29] P. R. Troyk, M. Edgington, "Inductive links and drivers for remotely-powered telemetry systems", Antennas and Propagation Society International Symposium, 2000, IEEE, Vol. 1, 16-21 July 2000, pp. 60 – 62
- [30] C. M. Zierhofer and E. S. Hochmair, "Coil design for improved power transfer efficiency in inductive links", Proceedings of the 18th Annual International Conference of the IEEE Engineering in Medicine and Biology Society, 1996. Bridging Disciplines for Biomedicine, Vol. 4, 31 Oct.-3 Nov. 1996, pp. 1538 – 1539.
- [31] M. Suster, D.J Young, W.H. Ko, "Micro-power wireless transmitter for high-temperature MEMS sensing and communication applications", The Fifteenth IEEE International Conference on Micro Electro Mechanical Systems, 2002, 20-24 Jan. 2002, pp. 641 -644
- [32] D. Azzi, G.S. Virk, "Wireless temperature sensing for building management systems", IEE Colloquium on Wireless Technology (Digest No. 1996/199), 14 Nov. 1996, pp. 2/1-2/4
- [33] L. A. Glasser, A. C. Malamy, C. W. Selvidge, "A magnetic power and communication interface for a CMOS integrated circuit", IEEE Journal of Solid-State Circuits, Vol. 24, Issue 4, Aug. 1989, pp. 1146 – 1149.
- [34] S.C.Q. Chen, V. Thomas, "Optimization of inductive RFID technology", Proceedings of the 2001 IEEE International Symposium on Electronics and the Environment, 7-9 May 2001, pp. 82 – 87.
- [35] Active and Passive RFID: Two distinct, But Complementary, Technologies for Real-Time Supply Chain Visibility. A white paper by Savi Technology. January 2002. Website: [http://www.savi.com/solutions/whitepapers/RFID\\_whitepaper.pdf](http://www.savi.com/solutions/whitepapers/RFID_whitepaper.pdf)

- [36] Active RFID: Selecting the Optimal Frequency for Global Applications. A white paper by Savi Technology. February 2002. Active Website: [http://www.savi.com/solutions/whitepapers/active\\_rfid.pdf](http://www.savi.com/solutions/whitepapers/active_rfid.pdf)
- [37] Carl T. A. Johnk, Engineering Electromagnetic Fields Waves, John Wiley & Sons, 1988.656 p.
- [38] E. H. Callaway, Jr., Wireless Sensor Networks: Architectures and Protocols, Auerbach publications. 2003. 342 p.
- [39] C. A. Balanis, Antenna Theory: Analysis and design, Second edition, John Wiley & Sons, 1996, 941p.
- [40] Hewlett-Packard Application Note1088, Designing the Virtual Battery.
- [41] C. M. Zierhofer and E. S. Hochmair, "Geometric approach for coupling enhancement of magnetically coupled coils", IEEE Transactions on Biomedical Engineering, Vol. 43, Issue 7, July 1996, pp. 708 – 714
- [42] C. M. Zierhofer, "A class-E tuned power oscillator for inductive transmission of digital data and power", Proceedings of 6th Mediterranean Electrotechnical Conference, 22-24 May 1991, pp. 789 - 792 vol.1
- [43] S. C. Cripps. RF power amplifiers for wireless communicaions. Artech House. 1999. 337p.
- [44] N. O. Sokal, A. D. Sokal, "Class-E, a new class of high-efficiency tuned single-ended switching power amplifiers", IEE Journal on Solid-State Circuits, Vol. SC-10, no. 3, June 1975, pp. 168 – 176.
- [45] F. H. Raab, "Idealized Operation of the Class-E Tuned Power Amplifier", IEEE Transactions on Circuits Systems, Vol. CAS-24, pp. 725–735, December 1977.
- [46] M. K. Kazimierczuk, K. Puczko, "Exact analysis of class E tuned power amplifier at any Q and switch duty cycle", IEEE transactions on Circuits and Systems, Vol. 34, No. 2, pp. 149-159, 1987.
- [47] M. A. K. Schwan and P. R. Troyk, "High efficiency driver for transcutaneously coupled coils", Proceedings of the Annual International Conference of the IEEE Engineering in Medicine and Biology Society, 1989. Images of the Twenty-First Century, 9-12 Nov. 1989, pp.1403 – 1404.
- [48] P. R. Troyk and M. A. K. Schwan, "Closed-Loop Class-E Transcutaneous Power and Data Link for MicroImplants", IEEE Transactions on Biomedical Engineering, vol. 39, pp. 589–599, June 1992.
- [49] N. O. Sokal, "Class-E RF power amplifiers ... ", QEX, No. 204, pp. 9-20, Jan./Feb. 2001.

- [50] K. G. Ong, C. A. Grimes, C. L. Robbins, and R. S. Singh, "Design and application of a wireless, passive, resonant-circuit environmental monitoring sensor", *Sensors and Actuators A* 93 (2001), pp. 33 – 43.
- [51] M. Rashid, *Microelectronic Circuits, Analysis and Design*. DWS Boston, 1999. 990p.
- [52] A. S. Sedra and K. C. Smith, *Microelectronic Circuits, Fourth Edition*, Oxford University Press, 1998, 1237pp.
- [53] Multilayer Ceramic Chip Capacitor (For general electronic equipment). Technical document. Panasonic. Website: <http://www.panasonic.com>. Active March 2004.
- [54] Ceramic Capacitors SMT Manual. PACCOM Electronics. Technical document. Website: <http://www.pacom.com/pacom/download/ceramics/mt-698.pdf>. Active March 2004.
- [55] National Semiconductor. LM 60, 2.7V SOT-23 or TO-92 IC Temperature Sensor Datasheet. Website: <http://cache.national.com/ds/LM/LM60.pdf>
- [56] Dallas Semiconductor – Maxim. Trimless IF VCO: Part 1: Design Considerations. Application Note 711.
- [57] Dallas Semiconductor – Maxim. Trimless IF VCO: Part 2: New ICs Simplify Implementation. Application Note 688.
- [58] W. Hayward, *Introduction to Radio Frequency Design*, The American Radio Relay League, Inc., 1994, 383p.
- [59] Dallas Semiconductor – Maxim. MAX2605-MAX2609 data sheet. Website: <http://pdfserv.maxim-ic.com/en/ds/MAX2605-MAX2609.pdf>
- [60] N. Demma, "Balanced Meissner Oscillator Circuit, RF Design, vol. December 1993, pp. 72-74.
- [61] AD654 Low Cost Monolithic Voltage-to-Frequency Converter. Datasheet. Website: [http://www.analog.com/UploadedFiles/Data\\_Sheets/76568190149713AD654\\_b.pdf](http://www.analog.com/UploadedFiles/Data_Sheets/76568190149713AD654_b.pdf)